Limnol. Oceanogr., 59(2), 2014, 603–622

doi:10.4319/lo.2014.59.2.0603

Modeling photoinhibition-driven bleaching in Scleractinian coral as a function of light, temperature, and heterotrophy

Malin S. M. Gustafsson,[1,*] Mark E. Baird,[2] and Peter J. Ralph [1]

[1] Plant Functional Biology and Climate Change Cluster, Faculty of Science, University of Technology, Sydney, Sydney, New South Wales, Australia

[2] Commonwealth Scientific and Industrial Research Organisation, Marine and Atmospheric Research, Hobart, Australia

Abstract

It has been proposed that corals with symbiotic algae (*Symbiodinium*) bleach under thermal stress due to temperature-dependent inactivation of the Rubisco protein that impairs CO_2 uptake, causing a backlog of electrons that result in the formation of damaging Reactive Oxygen Species. We present a numerical model of this mechanism of photoinhibition for symbiotic algae residing within coral tissue. The resulting rate of bleaching depended on temperature, light intensity, and the rate of heterotrophic feeding. The model was validated using three independently published experimental data sets. The model was capable of capturing both the diurnal change in the state of the photosystem, as well as changes in the symbiont population and the coral host caused by different temperature, light, and feeding treatments. Elevated temperatures and light led to a degradation of the photosystem and the expulsion of symbiont cells. If the coral fed heterotrophically, this degradation of the photosynthetic apparatus was reduced, but still a clear decrease in maximum quantum yield ($F_v : F_m$) and cell numbers was observed when the coral was exposed to elevated temperature. The reduction in chlorophyll content of cells at elevated temperatures and light was compared with the observational bleaching index Degree Heating Days (DHD). As quantified by DHD, the model was found to bleach under similar thermal stress regimes as field studies, except under elevated heterotrophic feeding conditions, which resulted in reduced severity of bleaching over a 90 d period.

Reef building corals (Scleractinian) live close to their observed upper thermal limit during summer months (Lesser and Farrell 2004). As a consequence of increasing sea-surface temperatures (SST), mass coral-bleaching events have become more frequent (Wilkinson 2002; Hughes et al. 2003). Most corals living in the photic-zone of the ocean are known to harbor symbiotic unicellular dinoflagellate algae from the genus *Symbiodinium* within their tissues. Coral bleaching is caused by a breakdown of the coral–algae symbiosis, resulting in the loss of photosynthetic pigments or expulsion of the algae symbionts from the coral host tissues (Brown 1997; Jones 2008).

The symbiotic relationship between the coral host and the symbiotic algae depends upon the autotrophic symbiont fixing carbon (C) through photosynthesis, which is used to synthesize products such as glycerol, glycerides, amino acids, and fatty acids (Falkowski et al. 1984; Muscatine 1990; Sutton and Hoegh-Guldberg 1990). Glycerol and glycerides can be produced in large quantities causing a high C : N ratio of photosynthetic products (Sutton and Hoegh-Guldberg 1990; Grant et al. 1997). These photosynthates can be translocated to the host, providing a source of nutrients (Wang and Douglas 1999). Additionally, the corals can feed on a wide range of prey items from zooplankton to particulate and dissolved organic matter (POM and DOM). Corals can capture prey items by tentacle grabbing, nematocyst discharges, or mucus adhesion (Houlbrèque and Ferrier-Pagès 2009). The metabolic byproducts of the host in turn provide the symbiont population with a steady supply of inorganic compounds, such as carbon dioxide, ammonium, urea, and polyphosphates (Titlyanov and Titlyanova 2002).

When the coral is exposed to elevated light and temperature, the photosystem of the symbiotic algae may become photoinhibited (Hoegh-Guldberg and Jones 1999; Venn et al. 2008). Photoinhibition may lead to damage to the photosystem and eventually bleaching due to oxidative stress, involving the production and accumulation of reactive oxygen species (ROS [Lesser 2006; Venn et al. 2008]). A physical trigger of photoinhibition is the temperature-induced breakdown of the Ribulose bisphosphate carboxylase oygenase (Rubisco) enzyme (Lilley et al. 2010). Rubisco is essential for the fixation of CO_2 for photosynthesis; if inactive, it causes a blockage of the electron transport chain (ETC) that leads to a build-up of electrons, which can react with O_2 to form superoxide (O_2^-) at the site of photosystem I (PSI; Venn et al. 2008). Superoxide dismutase catalyzes the reaction turning O_2^- of hydrogen peroxide (H_2O_2), whereas the detoxifying enzymes ascorbate peroxidases can reduce the H_2O_2 to water (Asada 2006). The production of O_2^- and H_2O_2 is called the Mehler reaction (Mehler and Brown 1952). In addition to the Mehler reaction, ROS can form as singlet oxygen ($^1O_2^*$), which is produced because of the highly reactive triplet states of chlorophyll (^{3}Chl) reacting with O_2. Triple excited Chl is a result of restricting the rate of the electron flow through the ETC causing maximal reduction of the plastoquinone, which causes a build-up of excess excitation energy (Jones et al. 1998).

Photosynthesis and cell respiration will continuously produce low levels of ROS, such as singlet oxygen ($^1O_2^*$), hydroxyl radical (OH^-), superoxide (O_2^-), and hydrogen

* Corresponding author: malin.gustafsson@student.uts.edu.au

peroxide (H_2O_2 [Asada 2006; Lesser 2006]). However, oxidative stress only occurs when the production of ROS exceeds the ability of the organisms to eliminate the ROS using cellular products such as antioxidants (Lesser 2006). Accumulated ROS may cause damage to the photosystem, as well as to both symbiont and host tissues (Asada 2006; Venn et al. 2008). The presence of highly ROS such as $^1O_2^*$, with an average lifetime of 3.7 μs, commonly results in specific damage to protein in close association with the site where the ROS was formed (Lesser 2006). As $^1O_2^*$ forms at PSII, it can prompt the degradation of the D1 protein (Asada 1996), as well as cause damage and bleaching of pigments in the light-harvesting complex (Venn et al. 2006). Other ROS such as H_2O_2, which is uncharged, have longer lifetimes and can therefore move across cell membranes to other parts of the algal cell or even into the host (Saragosti et al. 2010).

When a photon is absorbed by a Chl *a* molecule, it excites the chlorophyll from the ground state to the single excited state. The energy from the excited molecule may then have one of four fates: (1) the energy may be passed to the reaction center, in PSI or PSII, where it will be used for photochemical quenching (photosynthesis); (2) the energy can be dissipated as heat returning the chlorophyll molecule to the ground state (non-photochemical quenching); (3) the chlorophyll can re-emit the energy as a longer wavelength photon (fluorescence); or (4) as mentioned above, the chlorophyll excited state (Chl*) can be converted into a triplet spin configuration (^{3}Chl), which is a potent sensitizer of $^1O_2^*$; this process does not include any transfer of electrons but results in molecular damage (Apel and Hirt 2004).There are several additional sites within the symbiont and the host where ROS can form, such as the mitochondria (Dunn et al. 2012); however, in this study we focus on ROS production associated with the photosystem.

There are several protective mechanisms the algae may use to counteract or reduce the damaging effects of light and temperature stress, such as non-photochemical quenching and detoxification of ROS (Kirk 1994). Non-photochemical quenching (NPQ) involves the fast modification of auxiliary pigments to switch their photochemical function from light absorbing to heat dissipating under high light conditions and reverses under low light, and is referred to as the xanthophyll cycle. In dinoflagellates, the pigment diadinoxanthin is converted to diatoxanthin through the removal of an epoxy group under high light.

It has also been suggested that repair rates of the photosystem may be temperature-dependent; Hill et al. (2011) showed an up-regulation of D1 repair, whereas other studies showed a down-regulation (Hill et al. 2004; Murata et al. 2007; Takahashi et al. 2009). Similarly, the antioxidant activity may be up-regulated during elevated temperature (Flores-Ramírez and Liñán-Cabello 2007), yet this regulation varies between symbiont clades (McGinty et al. 2012).

The effect of elevated temperature on the coral symbiosis is linked to the D1 repair process and antioxidant systems, but it is also influenced by the host's ability to feed heterotrophically. An increased acquisition of nitrogen from heterotrophy has been shown to reduce photoinhibition and bleaching damage (Grottoli et al. 2006; Ferrier-Pagès et al. 2010; Hoogenboom et al. 2012). Heterotrophic feeding increased the host metabolism, hence supplying the symbiont with additional inorganic carbon and nitrogen and providing an additional source of energy that can be used to enhance the repair of damaged PSII. In addition, the host's need for translocated photosynthates decreases with increasing supply of heterotrophic food (Falkowski et al. 1984). An additional process that may be of importance, although not considered in this study, is the temperature-dependent changes in the microbial consortium associated with the coral (Gilbert et al. 2012).

The complexities associated with the dinoflagellate photosystem, and the processes leading to photoinhibition and coral bleaching, are still not fully understood. A process-based numerical model of this system may help to understand some of these complexities. Gustafsson et al. (2013) developed a coral symbiosis model, hereafter referred to as the GBR13 model, which described the symbiosis between an autotrophic algae symbiont and a heterotrophic cnidarian host under different light and nutrient conditions. The GBR13 model showed that being able to utilize both inorganic and organic sources of nutrients allowed for a stable host–symbiont population under low and variable nutrient fluxes. This model did not, however, include any temperature-dependence or sensitivity to high light of the symbiont photosystem and, thus, could not simulate the temperature- and light-dependent breakdown of the coral symbiosis that may lead to coral bleaching.

Here we present a numerical model of coral photosynthesis building upon the GBR13 model to simulate photoinhibition and subsequent bleaching. Evidence clearly indicates that the key trigger of thermal bleaching is the impairment of the photosystem (Venn et al. 2008). However, uncertainty remains concerning the sequence of events. There are three proposed effects of elevated temperature: energetic decoupling of the thylakoid membrane (Tchernov et al. 2004), impairment of the Calvin cycle through temperature-induced inactivation of Rubisco (Jones et al. 1998; Lilley et al. 2010), and dysfunction of PSII and degradation of the DI protein (Iglesias-Prieto et al. 1992). We chose to focus on the hypothesis that temperature-dependent inactivation of the Rubisco protein would impair the CO_2 uptake, causing a backlog of electrons that could result in the formation of ROS. This hypothesis was chosen because of the clear relationship between temperature and Rubisco activity and the availability of experimental data for model parameterization (Lilley et al. 2010).

The formation of $^1O_2$ through the excitation of chlorophyll was accounted for in the model because of the reduction of PSII, but was not given a separate state variable; rather, it was incorporated in the pool of ROS. In accordance with experimental studies, the ROS caused damage to the photosystem, as well as other cell tissues, if it was not eliminated by the antioxidant system or other detoxifying processes. Damaged PSII protein could be repaired, but when the photo-damage exceeded the repair rate, then photoinhibition occurred. A build-up of H_2O_2

Table 1. Assumptions made when deriving the model.

Temperature-dependent inactivation of Rubisco as the primary site affected by elevated temperatures.
Reactive oxygen is not transferred across cell membranes to the host.
Exocytosis: symbiont cells are expelled without causing damage to the host.
Translocation of photosynthates is influenced by the host's need of nutrient, a representation of the 'host release factor.'
Synthesis of new reaction centers (RCII) and xanthophyll pigments are assumed to occur at the same rate as chlorophyll synthesis.
The presence of three pigments was assumed: chlorophyll, diadinoxanthin, and diatoxanthin.

caused general tissue damage and expulsion of symbiont cells.

The model was fitted to the experimental photobiological data set of Hill et al. (2012) to derive the unknown parameters associated with D1 protein repair, detoxification and re-oxidation state of the photosystem. The model was assessed using the experimental ROS data from Suggett et al. (2008), and the effect of feeding vs. starvation on photoinhibition and bleaching were simulated and compared with the experimental data set by Borell and Bischof (2008). Finally, the temperature-dependence of bleaching in the model was compared with general field observations using the bleaching index Degree Heating Days (Maynard et al. 2008*a*), a tool used to predict onset and severity of coral bleaching.

Methods

The photoinhibition model developed in this paper builds on the coral symbiosis model of Gustafsson et al. (2013; hereafter, GBR13). The processes of nutrient cycling, respiration, cell division, mucus production, synthesis of tissues and chlorophyll, calcification, and more were based on the GBR13 model. One important alteration to the GBR13 model was redefining the translocation of photosynthates (T_C^S) from the symbiont to the host, where a new definition was needed:

$$T_C^S = \frac{(C_F^H(\mu_{\max}^H + \eta^H + \delta^H \mu_{\max}^H) - Z_C)\left(\frac{C_R^S}{C_{R,\max}^S}\right)}{S} \quad (1)$$

Where T_C^S is the translocation of carbon (C) from the symbiont to the host, $\mu_{\max}^H$ is the maximum host growth rate, η^H represents respiration and cell maintenance of the host, δ^H is the host C-specific cost of biosynthesis, Z_C is the rate of C acquisition through heterotrophic feeding, C_R^S is the symbiont C reserve, S is the number of symbiont cells, and $C_{R,\max}^S$ is the maximum size of the symbiont C reserve. Equation 1 replaces Eq. 4 in GBR13. This new definition resulted in a host-controlled translocation rate, where the host's need for energy set the rate, as long as the symbiont had sufficient energy to maintain its own cellular demands. The change was made to include the 'host factor'—a chemical agent present in the host tissues (Gates et al. 1995)—and is based on the observation that starved cnidarian hosts have been shown to extract a larger fraction of the newly produced photosynthates than fed hosts (Davy and Cook 2001).

The photoinhibition model described in this paper was linked to the GBR13 model, adding a much more detailed description of not just the photosystem, but also several associated processes such as antioxidant systems, and the nutritional cost of repairing the photosystem and producing antioxidants, as well as synthesis of diadinoxanthin and diatoxanthin pigments and the loss of symbionts due to damage caused by ROS production. However, not all processes of the photosystem were included because of our desire to constrain the complexity and because several of these processes are not yet fully understood. An example of such a process was the transfer of ROS from the symbiont cell to the host tissues and the host's ability to detoxify using its antioxidant system. We acknowledge that these processes will be important under some circumstances and should ideally be included into the model in the future. The major assumptions made deriving this model are stated in Table 1.

Model structure—The photoinhibition model described here included six new state variables (Fig. 1; Table 2), in addition to the ten described in GBR13 (Table 3). The first three new state variables included the different states of the photosystem defined as the number of reaction centers (RCII) per cell that were oxidized (Q_{ox}), reduced (Q_r), or inhibited (Q_i; Eqs. 3–5). Oxidized RCII (Q_{ox}) could pass the captured electron on through the ETC. However, one of the first steps in the ETC was the light-driven reduction of the primary acceptor plastoquinone in RCII, which was then balanced by its re-oxidation (Eqs. 3 and 4). The fourth and fifth state variables were the concentration of two xanthophyll pigments, diadinoxanthin (D_d), which could absorb photons and contribute to capturing light for photosynthesis, and diatoxanthin (D_t), which could dissipate heat; hence, it protected the cell when exposed to excessive light (Eqs. 6 and 7). The last state variable was the concentration of ROS formed after stress (RO_s; Eq. 8). This pool only contained ROS that had a relatively slow reaction rate, such as H_2O_2, because we assume that highly reactive ROS (such as $^1O_2^*$) would react with the surrounding tissues immediately; hence, they would not accumulate.

State variables from GBR13 that were altered during the coupling of the two models through the addition of a bleaching-associated loss term are redefined in the first part of Table 3 (Eqs. 9–12). The reduction term represented the energetic cost of repairing damage to the photosystem (B_{k_i}), as well as the cost of reducing ROS concentrations through detoxification ($B_{A_{RO}}$). The second half of Table 3 shows the state variables for the coral–algae symbiosis model presented in GBR13.

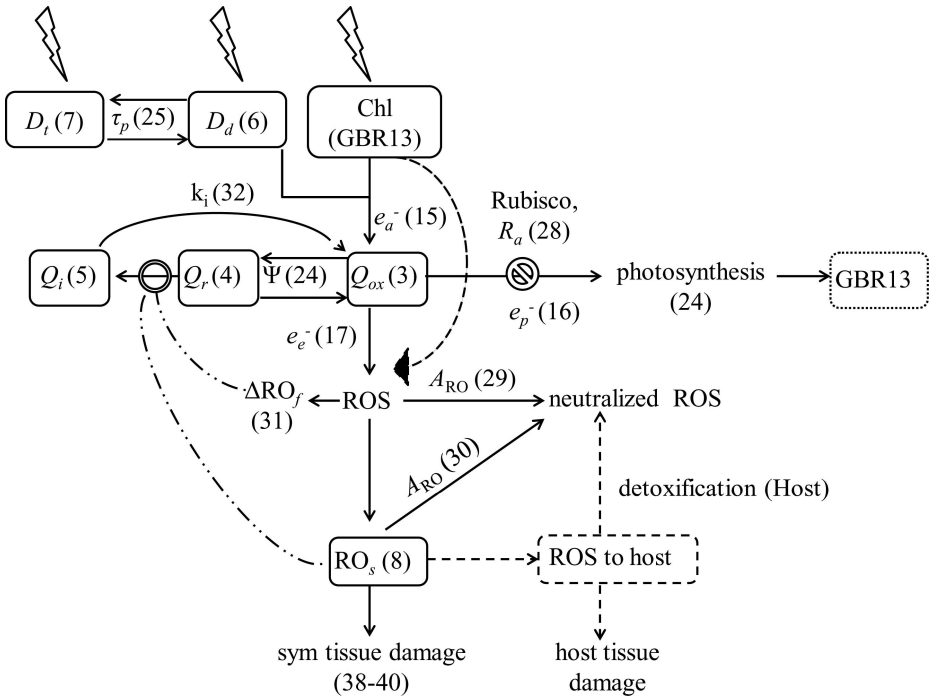

Fig. 1. Schematic of photoinhibition model; boxes indicate state variables and arrows are fluxes. ΔRO_f is not considered a state variable because we assume that it will immediately react with symbiont tissues at the site of formation, and hence inhibit the photosystem. The numbers in the brackets correspond to the equation number in Table 3. The dashed arrow and box referring to ROS in the host are not included in the model.

Figure 1 shows a schematic of the photoinhibition model. We go through each process shown in Fig. 1, as well as the process of calibrating the model to a data set collected by Hill et al. (2012), with an emphasis on deriving the unknown parameters, and as a means of using the model framework and observations to better describe these poorly understood processes. Model equations are presented in Tables 2–4 with associated parameters in Table 5, and relevant equations and parameters from GBR13 in Table 6 and 7.

Electron transport—For the purpose of this photoinhibition model, electron energy, which could be converted to ROS or C while moving through the model processes, were used as a form of model currency. The rate of electrons

Table 2. New state variable equations for the photoinhibition model. The number in brackets refers to the equation numbers used in the text.

Equation	Eq. No.	Description	Unit
$\frac{dQ_{ox}}{dt} = -\Psi - \Delta RO_f \frac{Q_{ox}}{Q_t} + k_i Q_i + \mu^{Chl} Q_t - \mu^S Q_{ox}$	(3)	oxidizes RCII	μmol RCII cell^{-1} d^{-1}
$\frac{dQ_r}{dt} = \Psi - \Delta RO_f \frac{Q_r}{Q_t} - \mu^S Q_r$	(4)	reduced RCII	μmol RCII cell^{-1} d^{-1}
$\frac{dQ_i}{dt} = \Delta RO_f \frac{Q_a}{Q_t} - k_i Q_i - \mu^S Q_i$	(5)	inhibited RCII	μmol RCII cell^{-1} d^{-1}
$\frac{dD_d}{dt} = \varsigma(D_d + D_t) - \tau_p - \mu^S D_d$	(6)	diadinoxanthin	μg D_d cell^{-1} d^{-1}
$\frac{dD_t}{dt} = \tau_p - \mu^S D_t$	(7)	diatoxanthin	μg D_t cell^{-1} d^{-1}
$\frac{dRO_s}{dt} = \begin{cases} f_{RO_s} RO - f_{RO_s} A_{RO} + \Delta RO_f \left(1 - \frac{Q_a}{Q_t}\right) - \beta RO_s - \mu^S RO_s & \text{if } I > 0 \\ -A_{RO} - \beta RO_s - \mu^S RO_s & \text{elsewhere} \end{cases}$	(8)	slow ROS	μmol ROS cell^{-1} d^{-1}

Table 3. State variable equations from the GBR13 model, where Eqs. 9–12 include the alterations made for this model. Equation numbers are given in brackets, and equation numbers following GBR13 indicate which equation it refers to in Gustafsson et al. (2013).

Equation	Eq. No.	Description	Unit
$\frac{dN_F^S}{dt} = \begin{cases} V_N^S - R_N^S - T_N^S - mN_F^S - \mu^S N_F^S - B_N^S & \text{if } \mu^S > 0\ N_F^S > N_{F,\max}^S \\ V_N^S - R_N^S - T_N^S - mN_F^S - \delta_N^S & \text{elsewhere} \end{cases}$	(9)	change in N_F^S	μg N cell^{-1} d^{-1}
$\frac{dC_F^S}{dt} = \begin{cases} V_C^S - R_C^S - T_{CF}^S - mC_F^S - \mu^S C_F^S - B_{CF}^S & \text{if } \mu^S > 0\ N_F^S > N_{F,\max}^S \\ V_C^S - R_C^S - T_{CF}^S - mC_F^S - B_{CF}^S & \text{elsewhere} \end{cases}$	(10)	change in C_F^S	μg C cell^{-1} d^{-1}
$\frac{dC_R^S}{dt} = \begin{cases} P_{\text{cell}}\left(1 - \frac{C_R^S}{C_{R,\max}^S}\right) - V_C^S - mC_R^S & \text{if } \mu^S > 0\ N_F^S > N_{F,\max}^S \\ \quad - T_{CR}^S - \mu^S C_R^S - B_{CR}^S & \\ P_{\text{cell}}\left(1 - \frac{C_R^S}{C_{R,\max}^S}\right) - V_C^S - mC_R^S - B_{CR}^S & \text{elsewhere} \end{cases}$	(11)	change in C_R^S	μg C cell^{-1} d^{-1}
$\frac{dS}{dt} = \begin{cases} \mu^S S - mS - m_S^{exp} & \text{if } \mu^S > 0\ N_F^S > N_{F,\max}^S \\ -mS - m_S^{exp} & \text{else} \end{cases}$	(12)	change in symbiont population size	cell cm^{-2} d^{-1}
$\frac{d\text{Chl}}{dt} = \begin{cases} \frac{V_N^S}{Q_F^S}\Pi_{\max}^L \theta_{\max}^C \Omega\varphi\left(1 - \frac{\text{Chl}}{\text{Chl}_{\max}}\right) & \text{if } I > 0\ C_R^S > C_{\text{thres}}^S \\ \frac{V_N^S}{Q_F^S}\Pi_{\max}^L \theta_{\max}^C \left(1 - \frac{\text{Chl}}{\text{Chl}_{\max}}\right) & \text{if } I = 0\ C_R^S > C_{\text{thres}}^S \\ -R_m^S \theta^C S & \text{if } C_R^S = 0 \\ 0 & \text{elsewhere} \end{cases}$	GBR13 (29a)	change in symbiont chlorophyll	μg Chl cell^{-1} d^{-1}
$\frac{dN_F^H}{dt} = Z_N - R_N^H - M_N$	GBR13 (43)	change in host N_F^H	μg N cm^{-2} d^{-1}
$\frac{dC_F^H}{dt} = V_C^H - R_C^H - M_{CF}$	GBR13 (44)	change in host C_F^H	μg C cm^{-2} d^{-1}
$\frac{dC_R^H}{dt} = Z_C + T_C^S S - M_{CR} - V_C^H$	GBR13 (45)	change in host C_R^H	μg C cm^{-2} d^{-1}
$\frac{d\text{DIC}^H}{dt} = V_{\text{DIC}}^H + R_C^H + R_C^S S - P_{\text{cell}} S\left(1 - \frac{C_R^S}{C_{R,\max}^S}\right) - \frac{d\text{Calc}}{dt} - eq\text{DIC}^H$	GBR13 (46)	change in host DIC^H	μg C cm^{-2} d^{-1}
$\frac{d\text{DIN}^H}{dt} = V_{\text{DIN}}^H + R_N^H + S(R_N^S - V_N^S) - eq\text{DIN}^H$	GBR13 (47)	change in host DIN^H	μg N cm^{-2} d^{-1}

generated within the cell (e_a^-) depended on the cell's absorption cross-sectional area (σ'), light intensity (I), and the quantum efficiency of PSII (φ_{PSII} [Eq. 15; Table 4]). The electrons could pass through the ETC and contribute to photosynthesis, e_p^- (Eq. 16), or, if there was any downstream blockage or if e_a^- exceeds the maximum capacity of the electron transport ($e_{\max}^-$), the electrons were produced in excess (e_e^-), which was the first step toward the production of ROS (Eq. 17). The process described above corresponded to the Mehler reaction (Mehler and Brown 1952) and was defined in a way that there was always some formation of e_e^- and hence ROS; however, under low light and optimal temperatures, the antioxidant and repair systems in the model were able to counteract the production of the ROS. The parameter $e_{\max}^-$ was defined as the rate of electrons that could pass through the ETC given the maximum number of PSII reaction centers (RCII) per cell ($Q_{\max}$) present in the oxidized form and in the absence of any downstream blockages (Eqs. 18–20). To estimate $e_{\max}^-$, we assumed a maximum light intensity ($I_Q^{\max}$) where all electrons could pass through the ETC (Eq. 18). To determine the maximum electrons per RCII (Eq. 19), the maximum number of absorbed photons $\left(I_Q^{\max}\sigma'\varphi_{\text{PSII}}\right)$ was divided by $Q_{\max}$ (Eq. 20). $Q_{\max}$ was calculated assuming a linear relationship between chlorophyll concentration and the number of RCIIs, using a RCII : Chl ratio established for *Symbiodinium* by Suggett et al. (2008). Hence, $Q_{\max}$ was achieved when the chlorophyll concentration was at its maximum, which was defined as the chlorophyll concentration required to absorb > 95% of the light incident upon the cell.

Photon absorption and the xanthophyll cycle—There are several types of pigments present within the symbiont cell. Some, such as chlorophyll, absorb light and pass the photons on through the photosystem; whereas others, such as diatoxanthin, absorb light and dissipate it as heat. Including all of the details of pigments present in the symbiont cell and their respective functions in the model was not feasible. Therefore, we focused on the processes considered most important for photo-protection and photoinhibition, and only three pigments were described

Table 4. Photoinhibition model equations. The number in brackets refers to the equation numbers used in the text.

Equation	Eq. No.	Description	Unit
$Q_t = Q_{ox} + Q_r + Q_i$	(13)	total RCII	μmol RCII cell^{-1}
$Q_a = Q_{ax} + Q_r$	(14)	active RCII	μmol RCII cell^{-1}
$e_a^- = \sigma' \varphi_{\mathrm{PSII}} I$	(15)	electron absorption rate	μmol e$^-$ cell^{-1} d^{-1}
$e_p^- = min\begin{cases} e_a^- \dfrac{Q_{ox}}{Q_t} R_a \\ e_{\max}^- R_a \end{cases}$	(16)	electrons leading to C fixation	μmol e$^-$ cell^{-1} d^{-1}
$e_e^- = e_a^- - e_p^-$	(17)	electrons diverted from C fixation	μmol e$^-$ cell^{-1} d^{-1}
$e_{\max}^- = \Phi Q_t$	(18)	max. e transport rate	mol e$^-$ cell^{-1} d^{-1}
$\Phi = \dfrac{I_Q^{\max} \sigma' \varphi_{\mathrm{PSII}}}{Q_{\max}}$	(19)	max. e transfer per RCII	mol e$^-$ mol RCII^{-1} d^{-1}
$Q_{\max} = \mathrm{Chl}_{\max} \theta_{\mathrm{Chl}}^{\mathrm{RCII}}$	(20)	max. RCII per cell	μmol RCII cell^{-1}
$P = \mathrm{Chl} + D_d + D_t$	(21)	total pigment pool	μg P m^{-3}
$\sigma = \pi r^2 \left(1 - \dfrac{2(1-(1+2\gamma Pr)e^{-2\gamma Pr})}{(2\gamma Pr)^2}\right)$	(22)	absorption cross-section	m^2 cell^{-1}
$\sigma' = \sigma \dfrac{\mathrm{Chl} + D_d}{P}$	(23)	effective absorption cross-section	m^2 cell^{-1}
$P_{\mathrm{cell}} = min\begin{cases} P_C^{\max}\left(\dfrac{\mathrm{DIC}^H}{\mathrm{DIC}^H + k_{\mathrm{DIC}}}\right) \\ \theta_C^{e^-} e_p^- \left(\dfrac{DIC^H}{\mathrm{DIC}^H + k_{\mathrm{DIC}}}\right) \end{cases}$	(24)	photosynthetic rate	μg C cell^{-1} d^{-1}
$\tau_p = \begin{cases} D_d \alpha^X f_T^I & \text{if } I > 0 \\ -D_t \alpha^X (1 - R_a) & \text{elsewhere} \end{cases}$	(25)	switching between absorbing and heat dissipating xanthophylls pigments	μg D$_x$ cell^{-1} d^{-1}
$\Psi = \begin{cases} \dfrac{e_a^-}{\Phi} \dfrac{Q_{ox}}{Q_t} (1 - R_a) & \text{if } I > 0 \\ -Q_r \dfrac{Q_r}{Q_t} R_a & \text{elsewhere} \end{cases}$	(26)	reduction or oxidation of active RCII	μmol RCII cell^{-1} d^{-1}
$\mu^{\mathrm{Chl}} = \dfrac{d\mathrm{Chl}}{dt} / \mathrm{Chl}$	(27)	chlorophyll growth rate	d^{-1}
$R_a = 0.058(T - T_i) + 1$	(28)	active fraction of Rubisco	—
$\Delta\mathrm{ROS} = \dfrac{e_e^-}{\theta_{\mathrm{RO}}^{e^-}(R_a)}$	(29)	rate of ROS formed by e_e^-	μmol ROS cell^{-1} d^{-1}
$A_{\mathrm{RO}} = \Delta\mathrm{ROS}\left(\dfrac{N_F^S}{N_F^S + N_{\mathrm{thres}}^S}\right)\left(\dfrac{C_R^S}{C_{R,\max}^S}\right)$	(30)	rate of detoxification	μmol e$^-$ cell^{-1} d^{-1}
$\Delta\mathrm{RO}_f = \begin{cases} f_{\Delta\mathrm{RO}_f} \Delta ROS - f_{\Delta\mathrm{RO}_f} A_{\mathrm{RO}} & \text{if } I > 0 \\ 0 & \text{elsewhere} \end{cases}$	(31)	electrons that form fast ROS	μmol RO$_f$ cell^{-1} d^{-1}
$k_i = \begin{cases} \alpha_d^K f_T^I Q_i \dfrac{C_R^S}{C_R^S + k_D} & \text{if } I > 0 \\ \alpha_n^K Q_i \dfrac{C_R^S}{C_R^S + C_{\mathrm{thres}}^S} & \text{elsewhere} \end{cases}$	(32)	repair rate of Q_i to Q_{ox}	μmol RCII cell^{-1} d^{-1}
$B_{k_i} = k_i \omega_{\mathrm{D1}} f_\delta$	(33)	carbon cost of D1 repair	μg C cell^{-1} d^{-1}
$B_{A_{\mathrm{RO}}} = A_{\mathrm{RO}} \omega_A f_\delta$	(34)	carbon cost of antioxidant activity	μg C cell^{-1} d^{-1}
$B_{CF}^S = (B_{A_{\mathrm{RO}}} + B_{k_i})\left(1 - \dfrac{C_R^S}{C_R^S + k_B}\right)$	(35)	total cost of D1 repair and detoxification taken from C_F^S	μg C cell^{-1} d^{-1}
$B_{CR}^S = (B_{A_{\mathrm{RO}}} + B_{k_i})\left(\dfrac{C_R^S}{C_R^S + k_B}\right)$	(36)	total cost of D1 repair and detoxification taken from C_R^S	μg C cell^{-1} d^{-1}
$B_N^S = \delta_{CF}^S Q_F^S$	(37)	total cost of D1 repair and detoxification taken from N_F^S	μg N cell^{-1} d^{-1}
$m_C^{exp} = \beta \mathrm{RO}_s \theta_{\mathrm{RO}}^C \omega_C$	(38)	rate of C loss due to symbiont expulsion	μg C cell^{-1} d^{-1}

Table 4. Continued.

Equation	Eq. No.	Description	Unit
$m_S^{exp} = \frac{m_C^{exp}}{C_F^S} S$	(39)	rate of symbiont expulsion	cell cm^{-2} d^{-1}
$f_T^I = \left(\frac{I}{I_{\text{noon}}}\right)^{(1-R_a)}$	(40)	light- and temperature-dependent shape factor	—

as state variables in the model—chlorophyll *a* (Chl *a*) because it acts as the primary donor of electrons to the ETC, as well as diadinoxanthin and diatoxanthin because of their photo-protective role in the xanthophyll cycle (Falkowski et al. 2007).

Absorption of light (σI) was calculated in the same manner as in GBR13; however, there are now three pigments rather than one (Eq. 21). The absorption cross-section was calculated for all pigments (σ; Eq. 22) and then the absorption cross-section for the absorbing pigments Chl *a* and diatoxanthin (σ'; Eq. 23). The photosynthetic output was set to correspond to e_p^- as long as it did not exceed the maximum photosynthetic rate ($P_C^{\max}$; Eq. 24). $P_C^{\max}$ was set to be the amount of C needed to provide for symbiont maximum growth rate ($\mu_{\max}^S$), including respiration and cost of biosynthesis, because photosynthesis above this rate would be energy-inefficient (Table 6). The photosynthetic output was also limited by the availability of dissolved inorganic carbon (DIC) in the host tissue (Gattuso et al. 1999), represented by the bracketed term in Eq. 24.

The description of the xanthophyll cycle in the model captured the interchange of xanthophyll pigments to minimize the damage due to light stress or maximize photosynthetic activity under low light conditions (Eqs. 6 and 7). The rate at which the xanthophyll pigments converted from one pool to the other (τ_p) was assumed to be light-dependent and temperature-dependent (Havaux and Tardy 1996; Eq. 25). To achieve this light and temperature dependence we used the diurnal light and temperature function f_T^I (*see* section Model evaluation) derived from Hill et al. (2012) data set.

Reduction and re-oxidation of RCII—The rate of reduction and re-oxidation of Q_{ox} and Q_r, Ψ, was a function of the amount of light the RCII were exposed to, e_a^-, divided by the maximal capacity of the RCII to pass electrons through to the ETC (Φ; Eq. 26). This formulation means that increasing light resulted in increasing RCII reduction; hence, fewer electrons were able to pass through to the ETC, reducing the potential production of ROS. The current oxidative state of the RCII pool ($Q_{ox}:Q_t$) was used to prevent Q_{ox} from ever becoming negative by slowing the reduction rate as Q_{ox} approached zero. The reduction-rate coefficients of Ψ (α_d^Q) and the temperature dependence of Ψ

Table 5. Description and value of model parameters.

Symbol	Description	Parameter value	Unit	Source
f_{RO_s}	fraction of ΔROS to RO$_S$ after detoxification	0.5	—	*see* text
$f_{\Delta\text{RO}_f}$	fraction of ΔROS to ΔRO$_f$ after detoxification	0.5	—	*see* text
β	reaction rate of RO$_S$ with symbiont tissues	3	d^{-1}	*see* text
$I_Q^{\max}$	max. I where all photons can pass through the ETC	500	μmol photon m^{-2} s^{-1}	Gorbunov et al. 2001
φ_{PSII}	quantum efficiency of charge separation at PSII	1	mol e$^-$ mol photon^{-1}	Ross et al. 2008
$\theta_C^{e^-}$	mol of electrons needed to make one mol of C	10	mol e$^-$ mol C^{-1}	Kirk 1994
$\theta_{\text{Chl}}^{\text{RCII}}$	RCII to Chl ratio	1.92×10^{-6}	mol RCII mol Chl^{-1}	Suggett et al. 2008
$T_{\max}$	temperature where Rubisco activity is zero	38	°C	Lilley et al. 2010
θ_{RO}^C	ROS-to-carbon ratio	1	mol C mol RO^{-1}	*see* text
I_{noon}	light intensity at midday	1500(600)	μmol photon m^{-2} s^{-1}	Borell and Bischof 2008; Hill et al. 2012
k_B	half-saturation constant for energy requirement of repair and detoxification of the photosystem	$10C_{\text{thres}}^S$	μg C cell^{-1}	—
k_{DIC}	half-saturation constant for DIC uptake by symbiont	0.5	pg C cell^{-1}	—
ω_{D1}	D1 molar mass	635	g C mol D1^{-1}	—
ω_A	antioxidant molar mass	120.1	g C mol D1^{-1}	—
ω_{C}	g C per mol C	12.01	g C mol C^{-1}	—
f_δ	fractional D1 repair cost of net D1 synthesis	0.008	—	Raven 2011
$\theta_{\text{RO}}^{e^-}$	mol of e$^-$ required to make mol ROS	7000	mol e$^-$ mol RO^{-1}	*see* text
α^X	xanthophyll conversion rate coefficient	1	d^{-1}	*see* text
α_d^Q	temperature-dependent reduction coefficient day	144	d^{-1}	*see* text
α_d^K	temperature-dependent repair coefficient day	$(47T-1151)(\times2.3)$	d^{-1}	*see* text
α_n^K	temperature-dependent repair coefficient day	0.001	d^{-1}	*see* text
T_i	temperature below which Rubisco activity is 100%	24	°C	Lilley et al. 2010

Table 6. Equations from Gustafsson et al. (2013; GBR13) relevant to this photoinhibition model. The numbers in brackets refers to the equation numbers in GBR13.

Symbol	Eq. No.	Description	Unit
$R_N^S = \begin{cases} V_N^S \eta^S + \delta^S N_F^S & \text{if } C_{\text{thres}}^S > 0 \\ \delta^S N_F^S & \text{elsewhere} \end{cases}$	(1)	cost of biosynthesis and respiration symbiont (N)	μg N cell^{-1} d^{-1}
$R_C^S = \begin{cases} V_C^S \eta^S + \delta^S C_F^S & \text{if } C_{\text{thres}}^S > 0 \\ \delta^S C_F^S & \text{elsewhere} \end{cases}$	(2)	cost of biosynthesis and respiration symbiont (C)	μg C cell^{-1} d^{-1}
$R_N^H = \begin{cases} V_N^H \eta^H + \delta^H N_F^H & \text{if } C_{\text{thres}}^H > 0 \\ \delta^H N_F^H & \text{elsewhere} \end{cases}$	(38)	cost of biosynthesis and respiration host (N)	μg N cm^{-2} d^{-1}
$R_C^H = \begin{cases} V_C^H \eta^H + \delta^H C_F^H & \text{if } C_{\text{thres}}^H > 0 \\ \delta^H C_F^H & \text{elsewhere} \end{cases}$	(39)	cost of biosynthesis and respiration host (C)	μg C cm^{-2} d^{-1}
$mN_N^S = m^S \mu_{\max}^S N_F^S$	(9)	mortality N_F^S	μg N cell^{-1} d^{-1}
$mC_F^S = m^S \mu_{\max}^S C_F^S$	(10)	mortality C_F^S	μg C cell^{-1} d^{-1}
$mC_R^S = m^S \mu_{\max}^S C_R^S$	(11)	mortality C_R^S	μg C cell^{-1} d^{-1}
$M_C = C_R^H \left(\frac{C_R^H}{C_{R,\max}^H} \right)$	(34)	total mucus C	μg C cm^{-2} d^{-1}
$M_N = \beta_N N_F^H$	(35)	N in mucus	μg N cm^{-2} d^{-1}
$M_{CF} = \beta_N N_F^H / Q_F^H$	(36)	C from C_F^H to mucus	μg C cm^{-2} d^{-1}
$M_{CR} = M_C - M_{CF}$	(37)	C from C_R^H to mucus	μg C cm^{-2} d^{-1}
$\mu^S = \frac{dC_F^S}{dt} / C_F^S$	(25)	symbiont growth rate	d^{-1}
$C_{\text{thres}}^S = ((L-24)/24) R_C^S$	text	symbiont C requirement to last through one night	μg C cell^{-1}
$C_{R,\max}^S = N_F^S / Q_{\min}^S - C_F^S$	(3)	max. size of C_R^S	μg C cell^{-1}
$S_{\max} = A_{\text{coral}} / \pi \left(3 \frac{N_F^S}{\rho} / 4\pi^{1/3} \right)^2$	(21)	max. number of symbiont cells per unit surface area	cell cm^{-2}
$P_C^{\max} = \mu_{max}^S \left(\frac{24}{L} \right) (1 + (\eta^S + \delta^S)) C_F^S$	(17)	max. C specific photosynthesis	μg C cell^{-1} d^{-1}
$V_{\text{DIC}}^H = \varepsilon_{\text{dic}} C_F^H \frac{\text{DIC}^E}{\text{DIC}^E + K_{\text{dic}}}$	(31)	host DIC uptake	μg C cm^{-2} d^{-1}
$eq\text{DIN}^H = \text{DIN}^H \left(\frac{\text{DIN}^H}{\text{DIN}_{\max}^H} \right)^4$	(32)	equilibration DIN in host	μg N cm^{-2} d^{-1}
$eq\text{DIC}^H = \text{DIC}^H \left(\frac{\text{DIC}^H}{\text{DIC}_{\max}^H} \right)^4$	(33)	equilibration DIC in host	μg C cm^{-2} d^{-1}
$V_{N,max}^S = \begin{cases} \mu_{\max}^S N_F^S \left[(1-\alpha) \left(\frac{24}{L} \right) + \alpha \right] & \text{if } I > 0 \\ \alpha \mu_{\max}^S N_F^S & \text{if } I = 0 \end{cases}$	(22)	max. N uptake by symbiont	μg N cell^{-1} d^{-1}
$V_N^S = V_{N,\max}^S \frac{\text{DIN}^H}{\text{DIN}^H + K_n} \left(\frac{C_R^S}{C_R^S + C_{\text{thres}}^S} \right) \left(1 - \frac{S}{S_{\max}} \right)$	(23)	actual N uptake rate by symbiont	μg N cell^{-1} d^{-1}
$\varphi = 1 - \frac{P_{\text{cell}}}{P_C^{\max}}$	(19)	regulatory term	—
$\Omega = \varphi \frac{\Pi_{\max}^L \theta_{\max}^C}{\theta^C}$	(20)	acceleration term	—

are described in the model evaluation section below. The rate of re-oxidation of Q_r to Q_{ox} was assumed to be able to oxidize the entire Q_r pool in 1 d if there was no temperature stress. In a similar manner to the reduction rate, the re-oxidation rate was reduced as Q_{red}: Q_t approached zero. In addition to the reduction and re-oxidation rate, there were other processes that could change the concentration of Q_{ox} and Q_r. Because of the limited information about RCII synthesis, we assumed a linear relationship between the synthesis of new RCII and the rate of chlorophyll

Table 7. Parameters from Gustafsson et al. (2013; GBR13) relevant to this photoinhibition model.

Symbol	Description	Value	Source	Unit
$\mu^S_{\max}$	maximum specific symbiont growth rate	0.4	Domotor and D'elia 1986; Falkowski et al. 2007	d^{-1}
$\mathrm{Chl}_{\max}$	maximum chlorophyll concentration per cell	concentration where <95% light is absorbed		μg Chl $cell^{-1}$
$\mathrm{DIC}_{\max}$	maximum DIC concentration in host tissues	C^H_F	—	μg C cm^{-2}
δ^S, δ^H	symbiont, host C-specific respiration and maintenance rate	0.06	—	g C g C^{-1} d^{-1}
η^S, η^H	symbiont, host C-specific cost of biosynthesis	0.1	—	g C g C^{-1}
$Q^S_{\min}$	minimum N : C ratio in symbiont	0.05	Ross and Geider 2009	g N g C^{-1}
L	No. daylight hours	12	—	h
A_{coral}	coral surface area	1	—	cm^2
α	factor by which dark N uptake rate is reduced	0.55	Ross and Geider 2009	—
K_n	half-saturation constant symbiont DIN uptake	1.4	Muscatine and D'elia 1978	μmol N L^{-1}
Z_N	N, C uptake rate by heterotrophic feeding	—	input parameter	μg cm^{-2} d^{-1}
$\varepsilon_{\mathrm{dic}}$	C-specific DIC uptake rate by host	6	Muller et al. 2009	g C g C^{-1} d^{-1}
K_{dic}	half-saturation constant host DIC uptake	400	Al-Moghrabi et al. 1996	μmol C L^{-1}
β_N	fraction of host N released as mucus	0.05	Bythell and Wild 2011	—
$\Pi^L_{\max}$	maximum proportion of C^S_F allocated to light harvesting	0.33	Ross and Geider 2009	—
$\theta^C_{\max}$	maximum Chl : C ratio of light harvesting pool	0.265	Ross and Geider 2009	g Chl g C^{-1}

production (Eq. 27). The chlorophyll synthesis was adapted from Ross et al. (2008). Newly synthesized RCII were incorporated into the Q_{ox} pool, as represented in the second last term in Eq. 3. The last term in all the new state variables represents the reduction per cell in the density of components of the photosystem due to cell division (Eqs. 3–8).

Reactive oxygen production—When temperature increased, the amount of active Rubisco decreased (Eq. 28), causing a reduction of electrons able to pass through the ETC leading to a build-up of excess electrons (e^-_e). The process of the formation of triplet excited ^{3}Chl was not included as a separate mechanism in the model. However, absorbed photons that did not pass through the RCII because of reduction or inhibition of Q_{ox} were assumed to excite Chl, causing the production of $^1O^*_2$; hence, all electrons absorbed but not used for photosynthesis became in excess (e^-_e) and contributed to ROS production (Eq. 29). The ROS could have one of three fates: (1) it could be detoxified and be neutralized (Eq. 30); (2) it could form fast ROS (ΔRO_f), which were assumed to be highly reactive and therefore causing immediate damage to the photosystem (Eq. 31); or (3) it could form long-lived slow ROS (RO_S), with a slower reaction rate, which could accumulate in the symbiont's tissue and potentially react with any part of the cell, causing structural damage and cell death (Eq. 8) (Apel and Hirt 2004). The fast ROS was formed near the RCII; therefore, the assumption was made that it primarily caused damage to the RCII, resulting in a pool of inhibited RCII (Q_i). This corresponds to the breakdown of the D1 protein rendering the reaction center inoperable until it is repaired. This damage to the photosystem was represented by the second term in Eqs. 3 and 4; if Q_{ox} or Q_r were approaching zero, the rate of Q_i formation would decrease.

Photosystem repair—An active repair rate (k_i) regenerated D1 protein and converted Q_i back to the Q_{ox} pool (Eq. 32). The repair rate, k_i, was set to depend upon light intensity, temperature, the size of the Q_i, and the size of the symbiont N and C pools. The temperature-dependent photosystem repair-rate coefficients (α^K_d and α^K_n) were derived by fitting the model to the Hill et al. (2012) data set (*see* section: Model evaluation). These up-regulating responses to light and temperature were reduced with decreasing N and C in the symbiont cell (Hill et al. 2011). Repairing the photosystem came at an energetic cost, set to be 1% of the total C requirement needed to synthesize a new D1 protein (Raven 2011; Eq. 33).

Rubisco activity—Temperature-dependent de-activation of the Rubisco enzyme caused a reduction in the sink of electrons by passing through the ETC. The de-activation of Rubisco was described by Lilley et al. (2010) to be strongly temperature-dependent; and by fitting a simple model to their data, we estimated the Rubisco activity (R_a) as a function of temperature (Eq. 28). Note, that the active fraction of Rubisco was used instead of an actual estimate of the Rubisco concentration in the cell.

Antioxidant activity—The ability of the antioxidant system to neutralize ROS is still not fully understood and quantitative measurements are generally not available; therefore, we decided to model antioxidant as a detoxification rate (A_{RO}) dependent upon the rate of ROS production and limited by the N and C required to maintain the detoxification process (Eq. 30). This detoxification term included all sinks of excess electrons reducing the formation of ROS, such as photorespiration and alternative electron transport paths. During daytime, the antioxidant system was assumed to neutralize the newly

formed ROS irrespective of species; the ROS remaining after detoxification was split into the fast and slow pool. During the night, there was no new formation of ROS and the fast pool was assumed to have completely reacted, leaving only the slow pool. As with the cost of photosystem repair, the detoxification process also had a cost set to be 1% of the total C cost of synthesizing a new antioxidant (Eq. 34).

Bleaching—The portion of ROS that was not detoxified was assumed to have reacted with the surrounding symbiont tissue and damaged it (Eq. 38). The model assumed a one-to-one ratio of RO_S to damage functional C. The rate of cell death due to ROSs was set to be the rate of C destruction over the size of the functional C pool (Eq. 39). Cell death caused by ROS or natural mortality was assumed to be lost, and the symbiont cell expelled from the coral tissue (Gates et al. 1992). The expulsion of the cells were assumed to occur through the release of isolated symbiont cells (exocytosis), a process assumed to occur without the release of any host tissue (Steen and Muscatine 1987). This assumption should be considered with care because it has been shown that under thermal stress the expulsion of symbiont cells often involved the release of the entire host endoderm cells encasing the symbionts (Gates et al. 1992). The decision to not include this potential damage to the host was made on the basis of constraining the complexity of the model.

Model evaluation—Hill and colleagues produced a data set using three coral species and two temperature levels (25°C and 31°C). Coral specimens used in Hill et al. (2012) were incubated in these two temperature treatments for 2 d, chlorophyll fluorescence measurements were taken at 05:00 h, 09:00 h, 13:00 h, 17:00 h, and 21:00 h each day, from which they calculated maximum quantum yield ($F_v : F_m$), effective quantum yield (Y(II)), non-photochemical quenching yield (Y(NPQ)), and non-regulated heat dissipation (Y(NO)). The experiment was conducted outdoors, so a natural light curve with a maximum of ~ 1500 μmol photon m^{-2} s^{-1} was used. The photoinhibition model was fitted to the data set for one of the three coral species, *Pocillopora damicornis*. This species was preferred because the GBR13 model was parameterized for this species where possible. To replicate the conditions for the experiment conducted by Hill et al. (2012), a similar light field was created using the latitude where the experiment was conducted and the time of year giving a maximum light intensity of 1500 μmol photon m^{-2} s^{-1} (Fig. 2A).

The photosystem repair rate, reduction and re-oxidation rates, and the rate of ROS production and detoxification are still not fully understood or agreed upon in the literature. These rates are likely to be temperature-dependent (Hill et al. 2012; McGinty et al. 2012). However, because there were no specific measurements of these rates or the effect of temperature, a temperature-dependent day and night repair coefficient (α_d^K and α_n^K), a shape factor of diurnal variations in light and temperature (f_T^I), a reduction rate coefficient (α_d^Q), and a temperature-dependent function ($\theta_{RO}^{e^-R_a}$) accounting for alternative sinks of electron that may reduce the production of ROS (Eq. 27) were derived by fitting the model to the Hill et al. (2012) data set. This would not be the preferred method when specific data and knowledge of the rate were available; thus, these processes and rates should be considered with care and, in the light of new findings or empirical data, should be tested and perhaps reconsidered. In the following sections, these rates and coefficients are described individually.

The Rubisco activity (R_a) was used to account for temperature dependence of reduction and re-oxidation of RCII (Ψ), meaning that the rate of RCII reduction increased toward its maximum with increasing temperature to aid photo-protection during daytime (Eq. 26). For the same reason at night elevated temperature meant a slower re-oxidation rate. The temperature dependence of the reduction and re-oxidation of the RCII pool were necessary to achieve the variation between the two temperature treatments seen in Fig. 2C. After an iteration process of fitting the model to the Hill et al. (2012) data set, the adjustment of the photosystem to a new light or temperature level was assumed to be able to take place over 10 min, giving a rate coefficient (α_d^Q) of 144 d^{-1}.

To fit the modeled $F_v : F_m$ curves to the Hill et al. (2012) data set, a daytime temperature-dependent repair-rate coefficient (α_d^K) was derived. The repair-rate coefficient increased linearly with increasing temperature. The relationship was set to be linear because we only had two temperature levels to work from; however, it is unlikely that this relationship is linear for all temperatures and it should be revisited if a new, more extensive data set becomes available. The function f_T^I was created to be able to constrain the repair process, which is dependent on daily variations in light intensity and temperature. The repair rate of RCII did not need to be as high under low light conditions and temperature, because the rate of photo damage was reduced. The value of f_T^I ranged between 0 and 1, and had a daily shape similar to the light curve with a maximum of 1 at midday, but with the steepness of the curve depending on temperature (Eq. 40). The derived parameter f_T^I was calculated as the ratio of the current light level relative to the light level at midday and the exponential based on Rubisco activity, which determined the temperature component.

The process of ROS production is still the most uncertain process in the model; we could find essentially no quantitative data defining the process of ROS production. As mentioned above, the ROS production was reduced because we implicitly include processes, such as singlet oxygen being quenched by carotenoids, as well as a sink of electrons due to alternative electron transport paths, such as cyclic electron flow around PSII and photo-respiration (Ulstrup et al. 2006; Crawley et al. 2010). If all excess electrons were assumed to become ROS, the symbiont population became greatly damaged already at low light and temperature levels. The electron-to-ROS conversion function was formulated such that at low temperature and light stress the alternative electron sinks removed almost all excess electrons, and as stress increased the efficiency of alternative sinks eventually became limited.

The initial conditions used for the model was set to equal the Hill et al. (2012) data set at time zero (Table 8). The host parameterization was left unchanged from the GBR13

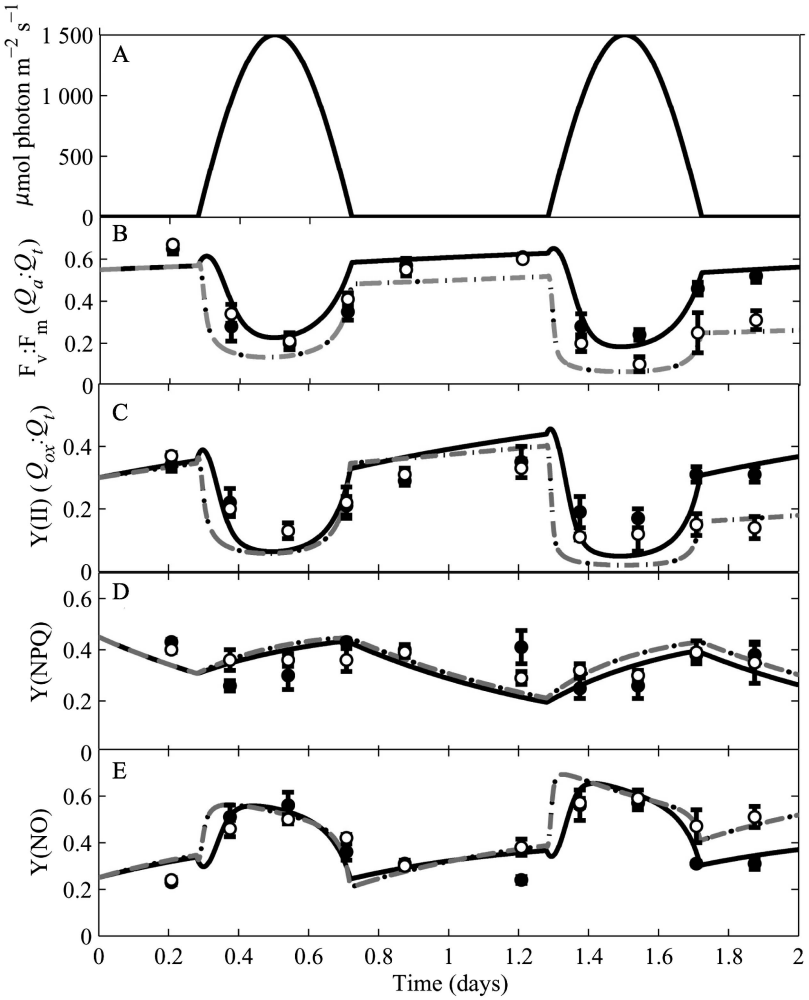

Fig. 2. Model fitted to data from Hill et al. (2012). Solid lines represented the 25°C model run over a 2 d period. Dashed line is the model run at 31°C. Filled markers indicate the experimental data for the 25°C treatment and open markers indicate the 31°C treatment with ± standard deviation (SD). (A) is diurnal light oscillation. (B) $F_v:F_m$ data with corresponding $Q_a:Q_t$ in the model. (C) Photochemistry Y(II) corresponding in model was $Q_{ox}:Q_t$. (D) Y(NPQ) corresponding in the model $D_t:(D_t + D_d + \text{Chl})$. (E) Y(NO) calculated using the assumption Y(II) + Y(NPQ) + Y(NO) = 1.

model. The model state variables were used to calculate the maximum quantum yield of PSII ($F_v:F_m$), effective quantum yield of PSII (Y(II)), non-photochemical quenching yield (Y(NPQ)), and non-regulated heat dissipation (Y(NO)), using the following assumption that Y(II) + Y(NPQ) + Y(NO) = 1.

From the model state, $F_v:F_m$ was defined as the maximum ability of the photosystem if all RCII in the active pool were oxidized ($F_v:F_m = Q_a:Q_t$). Y(II) represents the fraction of the photosystem that was capable of photosynthesis ($Q_{ax}:Q_t$), and Y(NPQ) was the fraction dissipating energy as heat through the xanthophyll cycle ($D_t:(D_t + D_d + Chl)$). Y(NO) was calculated using the assumption above (Y(NO) = 1 − Y(II) − Y(NPQ)).

Feeding simulations—It has been documented that heterotrophic feeding may limit the effect of elevated temperatures by reducing photoinhibition and subsequently lessening bleaching (Ferrier-Pagès et al. 2003; Borell et al. 2008; Hoogenboom et al. 2012). This photoinhibition model was connected to the GBR13 model that originally described the exchange of nutrient between the environment, host, and symbiont, simulating the effect of heterotrophic feeding; therefore, this provided an opportunity to further explore and validate both models. Borell and Bischof (2008) constructed a study where the importance of heterotrophic feeding was measured under thermal stress conditions. Borell and Bischof (2008) examined the bleaching susceptibility and photosystem activity of *Symbiodinium* in the Scleractinian coral *Sylophora pistillata* under thermal stress associated with daily temperature rise of 2°C to 3°C over a 10 d period, with a temperature increase from 28°C to 29°C just after dawn and a midday maximum of 32.5°C. The studied coral specimens were collected in July–August 2005

Table 8. Definition of state variables and initial conditions for *Pocillopora damicornis* and *Stylophora pistillata.* The initial values for the symbiont population size and pigment pools for *P. damicornis* were derived from Hill et al. (2012), whereas the initial total values of the RCII pools were estimated from Suggett et al. (2008) and divided into the three pools so that initial $F_v:F_m$ and Y(II) values corresponded with those in Hill et al. (2012). For *S. pistillata* the initial values were derived by spinning up the model for 2 d using a smaller symbiont cell size.

Symbol	Description	*P. damicornis* initial values	*S. pistillata* initial values	Unit
Q_{ox}	oxidized RCII	4.1×10^{-3}	0.0015	pmol RCII cell^{-1}
Q_r	reduced RCII	3.4×10^{-3}	0.002	pmol RCII cell^{-1}
Q_i	inhibited RCII	6.2×10^{-3}	0.0015	pmol RCII cell^{-1}
RO_S	'slow' ROS	0	0.1	pmol ROS cell^{-1}
D_d	diadinoxanthin	7.2	0.92	pg D_d cell^{-1}
D_t	diatoxanthin	0.8	2.07	pg D_t cell^{-1}
Chl	chlorophyll *a*	8	3	pg Chl cell^{-1}
S	symbiont population size	8.5×10^5	5.2×10^6	cell cm^{-2}

off Barang Lompo Island (05°03′S, 119°19′E) at 3 m depth. We aimed to recreate the results from their study to further evaluate and validate our model.

In order to switch the model from *P. damicornis* to *S. pistillata* only two parameter changes were required. The first change was that of symbiont cell radius (r_i), which was reduced to accommodate a larger number of cells in each cell layer (Lajeunesse et al. 2005). As defined in the GBR13 model, there were two one-cell-thick layers of host cells that can harbor symbionts; this gave a maximum number of symbiont cells per coral surface area. To be able to reach the number of symbiont cells recorded for *Stylophora pistillata,* r_i had to be reduced from 5 μm to 3 μm (changed from 10 μm to 6 μm diameter cells). Changing r_i changes the maximal amount of C, N, and chlorophyll that one cell could contain. Secondly, the repair rate coefficients α_d^k and α_n^k were doubled.

Photosystem repair is a vital process in the protection against bleaching, and it has been speculated that variations in the ability of different coral species to photo-repair underlies the difference in bleaching susceptibility (Takahashi et al. 2004, 2009; Ragni et al. 2010). In vitro bleaching 'sensitive' *Symbiodinium* have been shown to have a reduced photo-repair rate in comparison to 'tolerant' clades of *Symbiodinium* (Takahashi et al. 2009; Ragni et al. 2010). Although in situ measurements of photo-repair are still sparse, it has been shown that the *Symbiodinium* associated with the bleaching-tolerant *Porites astreoides* had a higher repair rate than *Symbiodinium* associated with the bleaching-sensitive *Monstastraea faveolata* (Hennige et al. 2011). No such information was found for *P. damicornis* or *S. pistillata* at the time of this study.

In the Borell and Bischof (2008) experiment, corals acclimated in the experimental tanks under non-stress and non-feeding conditions for 2 d prior to the experiment. To get the initial conditions of the model, we ran the model for 2 d under these conditions. The results after these 2 d were then used as the initial conditions of the temperature and feeding experiment (Table 8).

For the temperature experiment, the model was run for 10 d with a daily temperature fluctuation corresponding to that defined by Borell and Bischof (2008) with a maximum at midday of 32.5°C and a temperature after dawn of 29°C. The model was run twice—first with, and then without, heterotrophic feeding. The feeding rate used was adapted from Ferrier-Pagès et al. (2010) where *S. pistillata* was recorded to have a maximum mean feeding rate of 233 μg C cm^{-2} h^{-1}. Based on this feeding rate and that the coral were fed for 3 h in Borell and Bischof (2008), the daily mean rate of C uptake from heterotrophic feeding was calculated to be 698 μg C cm^{-2} d^{-1}.

As described in the GBR13, uptake of DIN and DIC from the surrounding water could be used by the symbiont binding it into organic material that could be translocated to the host, thus providing the host with an additional source of nutrients. The water in the experimental tanks was filtered (0.5 μm) oligotrophic seawater with a DIN concentration of < 0.3 μmol L^{-1}. Average daily DIN and DIC uptake rates by the host were approximated to be 3.3 μg N cm^{-2} d^{-1} and 17 μg C cm^{-2} d^{-1}, respectively (Marubini and Thake 1999). The experimental corals were taken from a 6 m depth and the light levels during the experiment were adjusted to correspond to the light field at this depth with a maximum of 600 μmol photon m^{-2} s^{-1}; therefore, the I_{noon} was set to this value when running the feeding simulations.

Results

The photoinhibition model was successfully coupled to the GBR13 coral host–symbiont growth model. After adjusting the parameters to represent *P. damicornis* as far as possible (Table 5), as well as deriving the three unknown rates (Ψ, k_i, and A_{RO}), the model behaved in accordance with the *P. damicornis* data set by Hill et al. (2012). Figure 2 shows the calculations of $F_v:F_m$, Y(II), Y(NPQ), and Y(NO) from the model, as well as the experimental data set. The model captured both the daily variation and the trend of the photosynthetic parameters over time of the two treatments (*see* Fig. 2). The photosystem recovered slowly during the night for both temperature treatments. However, the damage caused during the day exceeded the ability of the system to detoxify, so there was a net D1 loss, resulting in a decrease in the modeled $F_v:F_m$ and Y(II). For the 25°C treatment, a diurnal variation in $F_v:F_m$ was seen, but there were no overall degradation of the photosystem over the 2 d. The 31°C temperature treatment in addition to the daily fluctuation showed an overall

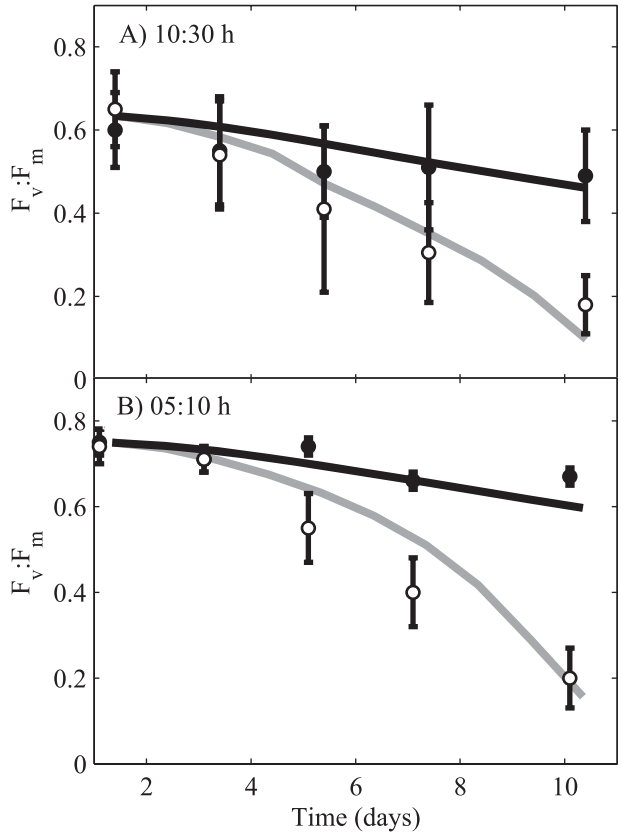

Fig. 3. $F_v:F_m$ at (A) 10:30 h and (B) 05:30 h for the modeled and Borell and Bischof (2008) experimental data during the 10 d feeding experiment. Closed and open markers show the measured $F_v:F_m$ for fed and unfed coral, respectively. Black and grey lines indicate the modeled $F_v:F_m$ ($Q_a:Q_t$) for fed and unfed coral, respectively.

degradation of the photosystem. There was an initial reduction in the modeled $F_v:F_m$ for the 31°C treatment relative to that seen in experimental data from the first day. The reason for this could be the presence of greater energy reserves in the experimental coral, which aids repair and delays onset of inhibition.

The modeled Y(NPQ) and Y(NO) also had a daily fluctuation, which increased during the daytime with a similar reduction during the night. The model showed only a small difference in Y(NPQ) and Y(NO) between temperature treatments, with the 31°C treatment being slightly higher and more so toward the end of the experiment.

Feeding simulations—After adjusting this model to fit Hill et al. (2012) and changing the initial conditions (Table 8), the Borell and Bischof (2008) data set could be simulated, showing that the two coupled models worked well together (Figs. 3, 4) for two different coral species. Similar to the Borell and Bischof (2008) data set, the model showed a greater reduction in $F_v:F_m$ for the starved coral than for the fed coral for both the 10:30 h and the 05:30 h measurement (Fig. 3). The 10:30 h measurements and model values were lower than those of the 05:30 h,

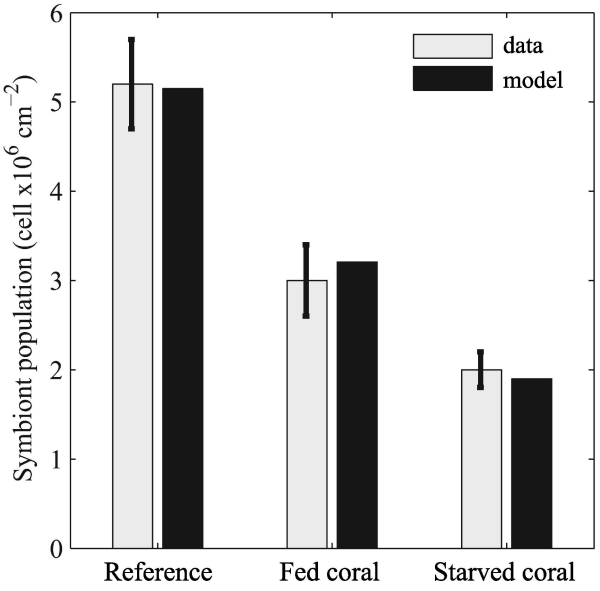

Fig. 4. Symbiont population size after 2 d acclimation under non-stress and non-feeding conditions (Reference) and after 10 d of elevated temperature for fed and starved corals. Light grey bar shows the measurements ± standard error (SE) from Borell and Bischof (2008).

indicating recovery of the photosystem during night. The model value at 05:30 h overlaid the Borell and Bischof (2008) data for the first 4 d. However, for the last day, the model calculated a $F_v:F_m$ value ~ 0.1 lower than the data for fed coral.

After running the model 10 d forward in time for the two treatments, the number of symbiont cells per coral surface area had decreased for both treatments to ~ 1.8×10^6 cell cm^{-2} and 3.28×10^6 cell cm^{-2} for the fed and starved coral respectively (Fig. 4). The model output corresponded well with the experimental results. The loss of symbionts in both the fed and unfed corals in the experiment was likely associated with elevation in temperature. In the model, this reduction in symbiont population (despite having a good supply of nitrogen [fed coral]) was found to be caused by the symbionts' maximum ability to repair and grow being exceeded by the rate of damage and natural mortality under these high temperature conditions.

Discussion

In this study, we developed a coral model that was able to simulate photoinhibition and the loss of the symbiont population due to temperature and light stress under different feeding regimes. The model captured both the diurnal change in the state of the photosystem, as well as overall degradation of the photosystem under temperature stress. Elevated temperatures led to a degradation of the photosystem and the loss of symbiont cells. If the coral could feed heterotrophically, this degradation was reduced, but still a decrease in the health of the photosystem was apparent (Fig. 3).

The dynamic rates derived by fitting the model to the Hill et al. (2012) data set probably represented more than one

actual physiological function each. For example, the A_{RO} (detoxification rate) that we presented as the activity of the antioxidant system probably also accounts for alternative electron paths and ROS scavengers (Asada 2006). Similarly the parameterization of the model accounts for the process of singlet oxygen formation from triple excited chlorophyll without defining it mechanistically. In the future, it would be ideal to resolve these rates with mechanistic formulations. Even so, the current model was able, with only a few parameter adjustments, to reproduce an independent experiment with a different species; this validates that this model does capture the main dynamic processes of coral symbiosis and its response to thermal and light stress.

Modeling all aspects of the photosystem would have been unnecessarily complex and probably not to be preferred because there are many functions and responses in the photosystem of which we still have limited understanding. However, one shortcoming of this model was that ROS could not move across the symbiont cell membrane into the host tissue. The choice to exclude this process was due to the lack of experimental data (Baird et al. 2009) and our wish to not incorporate any unnecessary uncertainty into the model. Similarly, the choice to use Rubisco activity, rather than having Rubisco content as a state variable changing over time, reduces the model complexity. Experimental data on Rubisco in *Symbiodinium* are scarce because Rubisco extracted from *Symbiodinium* has proved to be unstable, making quantitative measurements uncertain (Lilley et al. 2010).

An interesting outcome of this modeling study was that to get the model output to correspond to the Hill et al. (2012) data, k_i (the repair rate) had to be up-regulated with increasing temperature and light. This supports the finding by Hill et al. (2011), who found a significantly higher repair rate in corals exposed to temperature and light stress. They did not separate between light and temperature stresses, so a direct comparison of their rate constants was difficult. The need to up-regulate the repair rate was interesting because some researchers have found the opposite trend, with inhibition of the repair rate associated with increasing temperature (Murata et al. 2007; Takahashi et al. 2009).

The rather complex definitions of k_i and A_{RO} indicate that further experimental investigations of these rates are needed. The need to double the k_i rate for *S. pistillata* also suggests that these rates may be species- or clade-specific, as found by Henning et al. (2011) as well as McGinty et al. (2012).

H_2O_2 production—In this model, we assume that the ROS state variable, RO_S, corresponds to the accumulated H_2O_2 in the symbiont cell. Techniques to measure other ROS with faster reaction rates are still limited; however, H_2O_2 can be estimated using, for example, amplex red and horseradish peroxidase assays (Suggett et al. 2008). Suggett et al. (2008) provided a study of net H_2O_2 production in two different clades of cultured *Symbiodinium* for different light and temperature treatments. To establish whether the concentration of ROS produced by the model was reasonable, we ran the model using the experimental set-up of Suggett et al. (2008) with a 24 h temperature treatment (26°C and 32°C) prior to 1 h of light treatment (100 and 1000 μmol photon m^{-2} s^{-1}). The model was initiated using the same settings as we used to reproduce Hill et al. (2012). The conversion between ROS for the symbiont population and ROS per cell with a diameter of 12.5 μm was used. This conversion was made because cell size of cultured zooxanthellae has been found to be larger than the cell size of in hospite zooxanthellae (Domotor and D'elia 1986).

Figure 5 shows the modeled slow ROS (RO_S), as well as the results for the two *Symbiodinium* clades (A1 and B1) from Suggett et al. (2008). For both temperatures for the 100 μmol photon m^{-2} s^{-1} light treatments, the modeled RO_S concentration corresponded well with the measured values for both clades. Similarly, in the 32°C and 1000 μmol photon m^{-2} s^{-1} treatment, the model estimate lay within the standard deviation of clade A1. However, for the 26°C and 1000 μmol photon m^{-2} s^{-1} treatment, the modeled results differed notably from those measured, with modeled values close to those of the 100 μmol photon m^{-2} s^{-1} light treatment. The Suggett et al. (2008) study indicates that light intensity was a stronger inducer of H_2O_2 production than elevated temperature. This is not the case in the model; at optimal growth temperature, Rubisco activity is high and most captured energy will be used for photosynthesis. Additionally, the detoxification system effectively reduces the size of the RO_S pool. This divergence between the experimental data and the model indicates that the model definition may not capture all the dynamics of ROS production. As new measurements of ROS production in *Symbiodinium*, preferably in hospite, become available, this definition should be re-examined.

Degree heating days—Degree heating weeks (DHW) is a thermal stress index produced by the National Oceanic and Atmospheric Administration Coral Reef Watch. A few studies have use degree heating days (DHD) instead, which is a similar index but with a daily resolution (Maynard et al. 2008*a,b*). The DHD index uses sea-surface temperature (SST) to predict occurrence and severity of coral bleaching as a function of temperature anomalies that exceed the mean summer SST, as well as the duration of the elevated temperature:

$$\mathrm{DHD} = \sum_{i=1}^{n} (T_i - T_{\mathrm{mean}}) \quad (2)$$

Where T_{mean} is the mean climatological summer SST, T_i is the mean SST of day i, and n is the number of days. Two days with a temperature 2°C above T_{mean} has the same DHD as 1 d with a temperature 4°C above T_{mean}. The concept of DHD does not take into consideration the effect of other environmental conditions, such as light intensity, nutrient availability, or species-specific physiological properties such as photosystem repair. Field-derived relationships between bleaching and the DHD index provide a summary of field observations against which the photoinhibition model presented in this paper could be assessed.

To test the model's bleaching behavior at different values of the DHD index, the model was run for temperature scenarios 2°C, 3°C, and 4°C above T_{mean} for 90 d and a range of feeding rates and DIN uptake rates. The model

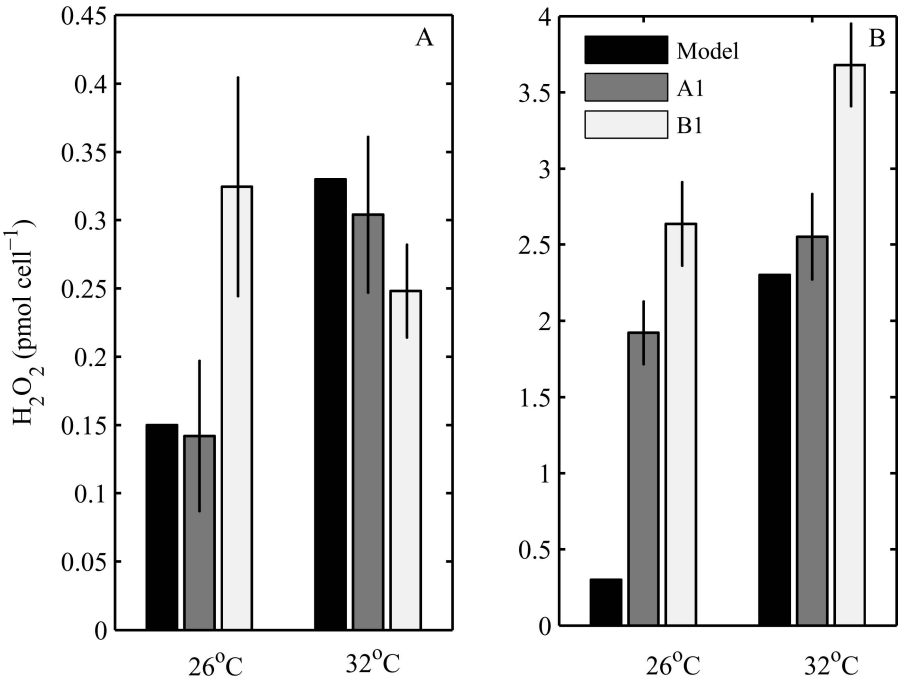

Fig. 5. Concentration of reactive oxygen species per symbiont cell (ROS) and H_2O_2 measurements (mean ± SE) from two *Symbiodinium* clades (A1 and B1) in culture, from Suggett et al. (2008). (A) 100 μmol photon m^{-2} s^{-1} treatment. (B) 1000 μmol photon m^{-2} s^{-1} treatment.

was forced using a light curve with a maximum intensity of 1000 μmol photon m^{-2} s^{-1} at noon and initiated with the values derived to initialize the model for the Borell and Bischof (2008) feeding experiment. These initial conditions were chosen to avoid any initial fluctuation of the model. The T_{mean} was set to 28°C. We acknowledge that the T_{mean} in the region where the coral for the Borell and Bischof (2008) study was located are likely to be closer to 30°C during summer; however, the corals were collected during July–August. The model was adjusted to the experimental conditions in Borell and Bischof (2008), where 28°C was the nighttime temperature under which the coral was able to maintain its biomass as long as food was available. We decided to use 28°C as T_{mean} because the modeled coral experienced damage above this temperature, and we worked under the assumption that T_{mean} should be close to the coral's upper thermal limit.

Figure 6 shows the percentage of initial chlorophyll pigmentation per coral surface area still remaining after exposure to elevated temperatures and varying heterotrophic nutrient input over time. Variation in DIN uptake did not reduce the severity of bleaching in the absence of heterotrophy. The model predicted that corals were almost entirely bleached after ~ 110–120 DHD irrespective of the DIN uptake rate in the absence of heterotrophy. Heterotrophy reduced the bleaching severity; however, this mitigating effect of feeding decreased with increasing temperature (Fig. 6). A model simulation at T_{mean} showed that at the highest feeding rates ~ 80% of the initial-condition chlorophyll concentration remains after 90 d, whereas the two lowest feeding rates approached zero (Fig. 6A). Interestingly, at a low heterotrophic feeding rate or at high temperature, complete bleaching occurred at the same thermal stress of ~ 110–120 DHD, as for the DIN simulations. Complete bleaching after 110–120 DHD was in agreement with literature (Maynard et al. 2008*a,b*). Maynard et al. (2008*a*) recorded complete or severe bleaching of three coral species after 120–140 DHD. However, the onset of bleaching seemed to occur somewhat earlier in the model than shown in Maynard et al. (2008*a*), where the bleaching severity at 50 DHD ranged between 5% and 40% of coral bleached. Note that there are likely to be great differences in stress across a reef, with varying light regimes and nutrient uptake, depending on location, current, and depth (Lesser et al. 2010; Wyatt et al. 2010). The light intensity used in this model simulation is that of a shallow reef (< 5 m), which may explain the earlier onset of bleaching in the model.

Coral bleaching is often referred to in terms of mild (< 25% bleached), moderate (< 50% bleached), and severe (> 50% bleached; Maynard et al. 2008*a*). The model output indicates that for the coral to only suffer mild to moderate bleaching during a prolonged heating event of 2°C above T_{mean}, the coral had to have a heterotrophic feeding rate of ~ 50 μg N cm^{-2} d^{-1} (Fig. 6B). This rate was only a fraction (~ 10%) of the calculated maximum coral feeding rate of 492 μg N cm^{-2} d^{-1} assuming that the coral mainly feed during the night and that the N : C of the ingested prey was at Redfield ratio (calculated from Ferrier-Pagès et al. [2010]). However, increasing the feeding rate above 50 μg N cm^{-2} d^{-1} had no further mitigating effect on bleaching. At 3°C above T_{mean} all simulations showed severe bleaching after ~ 50 DHD (Fig. 6C), and for the scenarios with 4°C

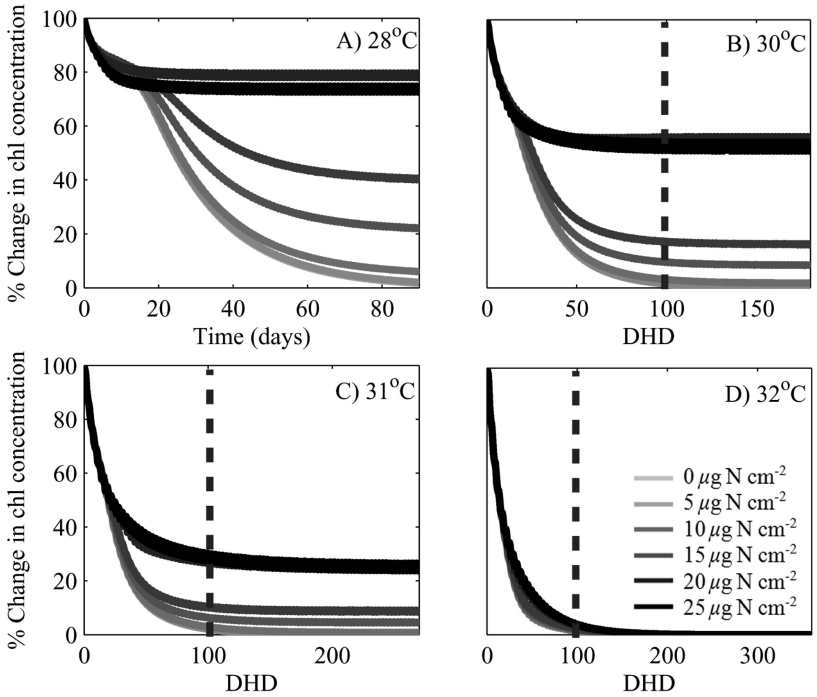

Fig. 6. Percentage of chlorophyll concentration remaining per coral-unit surface area as a function of heat stress and heterotrophic feeding over time. Vertical dashed lines indicate 100 DHD. (A) 90 d simulation at T_{mean} (28°C) for corals feeding heterotrophically at a range of rates. (B) 2°C above T_{mean}. (C) 3°C above T_{mean}. (D) 4°C above T_{mean}. Legend in panel D gives line shading for the heterotrophic feeding rates.

above T_{mean} all simulations were severely bleached after ~ 30 DHD.

The onset of bleaching was associated with a rapid loss of symbiont reserves (C_R^S) that in turn reduced the detoxifying and repair rate of the photosystem (Fig. 7). For the feeding rate of 100 μg N cm^{-2} d^{-1}, the RO_S pool increased as the C_R^S decreased, a result of ROS production exceeding detoxification and repair. The reason that C_R^S and the

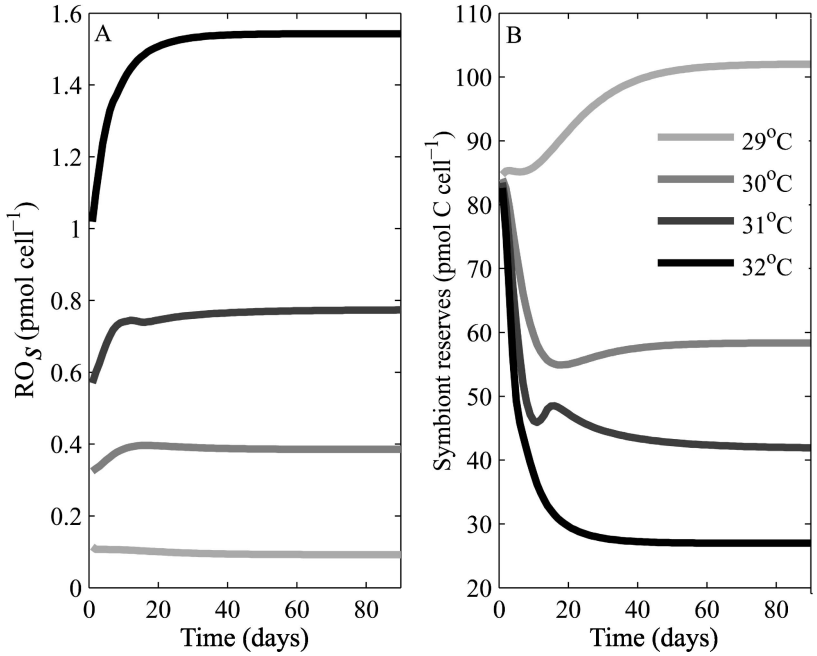

Fig. 7. (A) Concentration of ROS (RO_S) and (B) reserves (C_R^S) in the symbiont for T_{mean}, +2°C, +3°C, and +4°C heating over 90 d and a heterotrophic feeding rate of 100 μg N cm^{-2} d^{-1}.

concentration of RO_S for the 32°C scenario did not go to zero depends on the fact that the measurements were per cell and the population size still contained a few cells after 90 d (Fig. 7).

The reason that heterotrophic feeding delayed or prevented the depletion of the C_R^S pool was the fact that heterotrophically fed hosts did not need to extract photosynthates from the symbiont to the same extent as when only DIN was supplied. In the GBR13 model, it was shown that the host and symbiont both could survive under conditions where heterotrophy was low and DIN was high. This was not the case under temperature-stress conditions, because in addition to translocation to the host, more energy was also needed for photosystem repair and ROS detoxification.

The favorable comparison of the thermal stress behavior in the model and in field observations summarized using the DHD index gives some confidence that the model is capturing approximately the correct scale of thermal stress response in corals, and further that the mechanisms of photoinhibition and oxidative stress are important processes in coral bleaching.

The model highlights the importance of the coral being able to feed heterotrophically and the symbionts' ability to utilize host waste products. Previous studies have shown that under non-stress conditions, increasing DIN concentration in the environment may lead to increasing symbiont growth, as well as the ability to sustain the host when feeding is limited (Muller-Parker et al. 1994). However, corals under temperature stress have been found to have a reduced DIN uptake rate from the environment (Godinot et al. 2011). Additionally, elevated DIN concentrations in the water column have been found to increase symbiont expulsion rate (Zhu et al. 2004), and corals exposed to high DIN river run-off have been found to have a lower thermal tolerance threshold (Wooldridge and Done 2009). This lack of positive response from corals exposed to elevated DIN concentrations under heat-stress conditions supports the result presented here that DIN concentration had no effect on the bleaching rate. Also, in accordance with previous experiments, heterotrophy was found to have a mitigating effect on the bleaching rate (Borell et al. 2008; Connolly et al. 2012; Hoogenboom et al. 2012). We suggest that the reason that heterotrophy could reduce the effect of elevated temperatures but DIN could not was associated with a reduction in the translocation of photosynthates from symbiont to the host with increasing feeding rates, because of a reduction in the host need for an extra nutrient source. Hence, the symbiont was left with more reserves of nutrients, which it could use for cell maintenance, repair, and growth.

Overall, our model was found to respond to thermal stress in a similar manner as observed communities, as quantified by the DHD index. The model results and experimental studies suggest that adding a mitigating effect of an organic nutrient source may be a possible improvement in the prediction of coral bleaching. The difference in the onset of bleaching between the model and the data from Maynard et al. (2008*a*) may well be associated with the fact that we were using a model written to represent a single coral, or even a specific coral surface. Whereas, a coral reef usually contains several different species of coral in a range of local habitats with varying environmental conditions.

Future work—This photoinhibition model was used to reproduce several data sets, with only small adjustments to model settings that were required to account for different species as well as in hospite vs. cultured *Symbiodinium*, while still capturing the major responses to light intensity and temperature. However, because there are diverging theories as to how the photosystem responds to stress (Murata et al. 2007; Takahashi et al. 2008; Hill et al. 2011), further refinement of the model with the aim to pinpoint the reason behind diverging results from experimental studies would be useful. Resolving what we referred to as detoxification into antioxidant activity, photorespiration, and alternative electron pathways would be useful; and as experimental data become available, these components of the model should be updated. Likewise, transfer of ROS from the symbiont to the host and the ability of the host to deal with this additional source of ROS should also be incorporated into the model as soon as data become available. This model has the potential to be used for other symbiotic relationships between a heterotrophic host and an autotrophic symbiont, or it could be decoupled and used to look at free-living single-cell algae.

Acknowledgments

We thank Ross Hill, David Suggett, and Kai Bishof for providing experimental data for this paper. We thank the reviewers for their suggestions and comments, which helped to improve this manuscript.

We also thank the Australian Research Council (DP110105200) and the University of Technology, Sydney for providing funds for the University of Technology, Sydney President's Scholarship, and the International Postgraduate Research Scholarship.

References

Al-Moghrabi, S., C. Goiran, D. Allemand, N. Speziale, and J. Jaubert. 1996. Inorganic carbon uptake for photosynthesis by the symbiotic coral–dinoflagellate association II. Mechanisms for bicarbonate uptake. J. Exp. Mar. Biol. Ecol. **199:** 227–248, doi:10.1016/0022-0981(95)00202-2

Apel, K., and H. Hirt. 2004. Reactive oxygen species: Metabolism, oxidative stress, and signal transduction. Annu. Rev. Plant Biol. **55:** 373–399, doi:10.1146/annurev.arplant.55.031903.141701

Asada, K. 1996. Radical production and scavenging in the chloroplasts. Photosynthesis and the Environment **5:** 123–150, doi:10.1007/0-306-48135-9_5

———. 2006. Production and scavenging of reactive oxygen species in chloroplasts and their functions. Plant Physiol. **141:** 391–396, doi:10.1104/pp.106.082040

Baird, A., R. Bhagooli, P. Ralph, and S. Takahashi. 2009. Coral bleaching: The role of the host. Trends Ecol. Evol. **24:** 16–20, doi:10.1016/j.tree.2008.09.005

Borell, E. M., and K. Bischof. 2008. Feeding sustains photosynthetic quantum yield of a scleractinian coral during thermal stress. Oecologia **157:** 593–601, doi:10.1007/s00442-008-1102-2

———, A. R. Yuliantri, K. Bischof, and C. Richter. 2008. The effect of heterotrophy on photosynthesis and tissue composition of two scleractinian corals under elevated temperature. J. Exp. Mar. Biol. Ecol. **364:** 116–123, doi:10.1016/j.jembe.2008.07.033

Brown, B. E. 1997. Coral bleaching: Causes and consequences. Coral Reefs **16:** S129–S138, doi:10.1007/s003380050249

Bythell, J. C., and C. Wild. 2011. Biology and ecology of coral mucus release. J. Exp. Mar. Biol. Ecol. **408:** 88–93, doi:10.1016/j.jembe.2011.07.028

Connolly, S., M. Lopez-Yglesias, and K. R. Anthony. 2012. Food availability promotes rapid recovery from thermal stress in a scleractinian coral. Coral Reefs **31:** 951–960, doi:10.1007/s00338-012-0925-9

Crawley, A., D. I. Kline, S. Dunn, K. E. N. Anthony, and S. Dove. 2010. The effect of ocean acidification on symbiont photorespiration and productivity in *Acropora formosa*. Glob. Change Biol. **16:** 851–863, doi:10.1111/j.1365-2486.2009.01943.x

Davy, S. K., and C. B. Cook. 2001. The influence of 'host release factor' on carbon release by zooxanthellae isolated from fed and starved *Aiptasia pallida* (Verrill). Comp. Biochem. Physiol. Part A: Mol. Integr. Physiol. **129:** 487–494.

Domotor, S., and C. D'elia. 1986. Cell-size distributions of zooxanthellae in culture and symbiosis. Biol. Bull. **170:** 519–525, doi:10.2307/1541859

Dunn, S. R., M. Pernice, K. Green, O. Hoegh-Guldberg, and S. G. Dove. 2012. Thermal stress promotes host mitochondrial degradation in symbiotic cnidarians: Are the batteries of the reef going to run out? PLoS One **7:** e39024, doi:10.1371/journal.pone.0039024

Falkowski, P., Z. Dubinsky, L. Muscatine, and J. Porter. 1984. Light and the bioenergetics of a symbiotic coral. Bioscience **34:** 705–709, doi:10.2307/1309663

———, J. Raven, and E. Laws. 2007. Aquatic photosynthesis. Princeton Univ. Press.

Ferrier-Pagès, C., C. Rottier, E. Beraud, and O. Levy. 2010. Experimental assessment of the feeding effort of three scleractinian coral species during a thermal stress: Effect on the rates of photosynthesis. J. Exp. Mar. Biol. Ecol. **390:** 118–124, doi:10.1016/j.jembe.2010.05.007

———, J. Witting, E. Tambutté, and K. P. Sebens. 2003. Effect of natural zooplankton feeding on the tissue and skeletal growth of the scleractinian coral *Stylophora pistillata*. Coral Reefs **22:** 229–240, doi:10.1007/s00338-003-0312-7

Flores-Ramírez, L. A., and M. A. Liñán-Cabello. 2007. Relationships among thermal stress, bleaching and oxidative damage in the hermatypic coral, *Pocillopora capitata*. Comp. Biochem. Physiol. Part C: Toxicol. Pharmacol. **146:** 194–202.

Gates, R. D., G. Baghdasarian, and L. Muscatine. 1992. Temperature stress causes host cell detachment in symbiotic cnidarians: Implications for coral bleaching. Biol. Bull. **182:** 324–332, doi:10.2307/1542252

———, O. Hoegh-Guldberg, M. J. Mcfall-Ngai, K. Y. Bil, and L. Muscatine. 1995. Free amino acids exhibit anthozoan "host factor" activity: They induce the release of photosynthate from symbiotic dinoflagellates in vitro. Proc. Natl. Acad. Sci. **92:** 7430–7434, doi:10.1073/pnas.92.16.7430

Gattuso, J., D. Allemand, and M. Frankignoulle. 1999. Photosynthesis and calcification at cellular, organismal and community levels in Coral Reefs: A review on interactions and control by carbonate chemistry. Amer. Zool. **39:** 160–183.

Gilbert, J. A., R. Hill, M. A. Doblin, and P. J. Ralph. 2012. Microbial consortia increase thermal tolerance of corals. Mar. Biol. **159:** 1763–1771, doi:10.1007/s00227-012-1967-9

Godinot, C., F. Houlbrèque, R. Grover, and C. Ferrier-Pagès. 2011. Coral uptake of inorganic phosphorus and nitrogen negatively affected by simultaneous changes in temperature and pH. PLoS One **6:** e25024, doi:10.1371/journal.pone.0025024

Gorbunov, M. Y., Z. S. Kolber, M. P. Lesser, and P. G. Falkowski. 2001. Photosynthesis and photoprotection in symbiotic corals. Limnol. Oceanogr. **46:** 75–85, doi:10.4319/lo.2001.46.1.0075

Grant, A. J., M. Rémond, J. People, and R. Hinde. 1997. Effects of host-tissue homogenate of the scleractinian coral *Plesiastrea versipora* on glycerol metabolism in isolated symbiotic dinoflagellates. Mar. Biol. **128:** 665–670, doi:10.1007/s002270050133

Grottoli, A. G., L. J. Rodrigues, and J. E. Palardy. 2006. Heterotrophic plasticity and resilience in bleached corals. Nature **440:** 1186–1189, doi:10.1038/nature04565

Gustafsson, M. S. M., M. E. Baird, and P. J. Ralph. 2013. The interchangeability of autotrophic and heterotrophic nitrogen sources in Scleractinian coral symbiotic relationships: A numerical study. Ecological Modelling **250:** 183–194, doi:10.1016/j.ecolmodel.2012.11.003

Havaux, M., and F. Tardy. 1996. Temperature-dependent adjustment of the thermal stability of photosystem II in vivo: Possible involvement of xanthophyll-cycle pigments. Planta **198:** 324–333, doi:10.1007/BF00620047

Hennige, S. J., M. P. McGinley, A. G. Grottoli, and M. E. Warner. 2011. Photoinhibition of *Symbiodinium* spp. within the reef corals *Montastraea faveolata* and *Porites astreoides*: Implications for coral bleaching. Mar. Biol. **158:** 2515–2526, doi:10.1007/s00227-011-1752-1

Henning, S. J., P. G. Grottoli, and M. E. Warner. 2011. Photoinhibition of *Symbiodinium* spp. within the reef corals *Montastraea faveolata* and *Porites astreoides*: implications for coral bleaching. Marine Biology **158:** 2515–2526, doi:10.1007/s00227-011-1752-1

Hill, R., C. M. Brown, K. Dezeeuw, D. A. Campbell, and P. J. Ralph. 2011. Increased rate of D 1 repair in coral symbionts during bleaching is insufficient to counter accelerated photoinactivation. Limnol. Oceanogr. **56:** 139–146, doi:10.4319/lo.2011.56.1.0139

———, A. W. D. Larkum, C. Frankart, M. Kühl, and P. Ralph. 2004. Loss of functional Photosystem II reaction centres in zooxanthellae of corals exposed to bleaching conditions: Using fluorescence rise kinetics. Photosynth. Res. **82:** 59–72, doi:10.1023/B:PRES.0000040444.41179.09

———, ———, O. Prasil, D. M. Kramer, M. Szabo', V. Kumar, and P. J. Ralph. 2012. Light-induced dissociation of antenna complexes in the symbionts of scleractinian corals correlates with sensitivity to coral bleaching. Coral Reefs **31:** 963–975, doi:10.1007/s00338-012-0914-z

Hoegh-Guldberg, O., and R. J. Jones. 1999. Photoinhibition and photoprotection in symbiotic dinoflagellates from reef-building corals. Mar. Ecol. Prog. Ser. **183:** 73–86, doi:10.3354/meps183073

Hoogenboom, M. O., D. A. Campbell, E. Beraud, K. Dezeeuw, and C. Ferrier-Pagès. 2012. Effects of light, food availability and temperature stress on the function of photosystem II and photosystem I of coral symbionts. PLoS One **7:** e30167, doi:10.1371/journal.pone.0030167

Houlbrèque, F., and C. Ferrier-Pagès. 2009. Heterotrophy in tropical scleractinian corals. Biol. Rev. **84:** 1–17, doi:10.1111/j.1469-185X.2008.00058.x

Hughes, T., and others. 2003. Climate change, human impacts, and the resilience of coral reefs. Science **301:** 929–933, doi:10.1126/science.1085046

Iglesias-Prieto, R., J. Matta, W. Robins, and R. Trench. 1992. Photosynthetic response to elevated temperature in the symbiotic dinoflagellate Symbiodinium microadriaticum in culture. Proc. Natl. Acad. Sci. U. S. A. **89:** 10302–10305, doi:10.1073/pnas.89.21.10302

Jones, R. 2008. Coral bleaching, bleaching-induced mortality, and the adaptive significance of the bleaching response. Mar. Biol. **154:** 65–80, doi:10.1007/s00227-007-0900-0

———, O. Hoegh-Guldberg, A. Larkum, and U. Schreiber. 1998. Temperature-induced bleaching of corals begins with impairment of the CO_2 fixation mechanism in zooxanthellae. Plant Cell Environ. **21:** 1219–1230, doi:10.1046/j.1365-3040.1998.00345.x

Kirk, J. T. O. 1994. Light and photosynthesis in aquatic ecosystems, 2nd ed. Cambridge Univ. Press.

Lajeunesse, T. C., G. Lambert, R. A. Andersen, M. A. Coffroth, and D. W. Galbraith. 2005. *Symbiodinium* (Pyrrhophyta) genome sizes (DNA content) are smallest among dinoflagellates. J. Phycol. **41:** 880–886, doi:10.1111/j.0022-3646.2005.04231.x

Lesser, M. P. 2006. Oxidative stress in marine environments: Biochemistry and physiological ecology. Annu. Rev. Physiol. **68:** 253–278, doi:10.1146/annurev.physiol.68.040104.110001

———, and J. Farrell. 2004. Exposure to solar radiation increases damage to both host tissues and algal symbionts of corals during thermal stress. Coral Reefs **23:** 367–377, doi:10.1007/s00338-004-0392-z

———, M. Slattery, M. Stat, M. Ojimi, R. D. Gates, and A. Grottoli. 2010. Photoacclimatization by the coral Montastraea cavernosa in the mesophotic zone: Light, food, and genetics. Ecology **91:** 990–1003, doi:10.1890/09-0313.1

Lilley, R., P. J. Ralph, and A. W. D. Larkum. 2010. The determination of activity of the enzyme Rubisco in cell extracts of the dinoflagellate alga *Symbiodinium* sp. by manganese chemiluminescence and its response to short-term thermal stress of the alga. Plant, Cell Environ. **33:** 995–1004, doi:10.1111/j.1365-3040.2010.02121.x

Marubini, F., and B. Thake. 1999. Bicarbonate addition promotes coral growth. Limnol. Oceanogr. **44:** 716–720, doi:10.4319/lo.1999.44.3.0716

Maynard, J. A., K. Anthony, P. Marshall, and I. Masiri. 2008*a*. Major bleaching events can lead to increased thermal tolerance in corals. Mar. Biol. **155:** 173–182, doi:10.1007/s00227-008-1015-y

———, and others. 2008*b*. ReefTemp: An interactive monitoring system for coral bleaching using high-resolution SST and improved stress predictors. Geophys. Res. Lett. **35:** L05603, doi:10.1029/2007GL032175

McGinty, E. S., J. Pieczonka, and L. D. Mydlarz. 2012. Variations in reactive oxygen release and antioxidant activity in multiple *Symbiodinium* types in response to elevated temperature. Microb. Ecol. **64:** 1000–1007, doi:10.1007/s00248-012-0085-z

Mehler, A. H., and A. H. Brown. 1952. Studies on reactions of illuminated chloroplasts. III. Simultaneous photoproduction and consumption of oxygen studied with oxygen isotopes. Arch. Biochem. Biophys. **38:** 365–370, doi:10.1016/0003-9861(52)90042-8

Muller, E. B., S. a. L. M. Kooijman, P. J. Edmunds, F. J. Doyle, and R. M. Nisbet. 2009. Dynamic energy budgets in syntrophic symbiotic relationships between heterotrophic hosts and photoautotrophic symbionts. J. Theor. Biol. **259:** 44–57, doi:10.1016/j.jtbi.2009.03.004

Muller-Parker, G., C. Cook, and C. D'elia. 1994. Elemental composition of the coral *Pocillopora damicornis* exposed to elevated seawater ammonium. Pac. Sci. **48:** 234–246.

Murata, N., S. Takahashi, Y. Nishiyama, and S. I. Allakhverdiev. 2007. Photoinhibition of photosystem II under environmental stress. Biochim. Biophys. Acta – Bioenerg. **1767:** 414–421, doi:10.1016/j.bbabio.2006.11.019

Muscatine, L. 1990. The role of symbiotic algae in carbon and energy flux in reef corals. Ecosyst. World **25:** 75–87.

———, and C. D'elia. 1978. The uptake, retention, and release of ammonium by reef corals. Limnol. Oceanogr. **23:** 725–734, doi:10.4319/lo.1978.23.4.0725

Ragni, M., R. L. Airs, S. J. Hennige, D. J. Suggett, M. E. Warner, and R. J. Geider. 2010. PSII photoinhibition and photorepair in *Symbiodinium* (Pyrrhophyta) differs between thermally tolerant and sensitive phylotypes. Mar. Ecol. Prog. Ser. **406:** 57–70, doi:10.3354/meps08571

Raven, J. A. 2011. The cost of photoinhibition. Physiol. Plant. **142:** 87–104, doi:10.1111/j.1399-3054.2011.01465.x

Ross, O., and R. Geider. 2009. New cell-based model of photosynthesis and photo-acclimation: Accumulation and mobilisation of energy reserves in phytoplankton. Mar. Ecol. Prog. Ser. **383:** 53–71, doi:10.3354/meps07961

———, C. Moore, D. Suggett, H. MacIntyre, and R. Geider. 2008. A model of photosynthesis and photo-protection based on reaction center damage and repair. Limnol. Oceanogr. **53:** 1835–1852, doi:10.4319/lo.2008.53.5.1835

Saragosti, E., D. Tchernov, A. Katsir, and Y. Shaked. 2010. Extracellular production and degradation of superoxide in the coral *Stylophora pistillata* and cultured *Symbiodinium*. PLoS One **5:** e12508, doi:10.1371/journal.pone.0012508

Steen, R. G., and L. Muscatine. 1987. Low temperature evokes rapid exocytosis of symbiotic algae by a sea anemone. Biol. Bull. **172:** 246–263, doi:10.2307/1541797

Suggett, D. J., M. E. Warner, D. J. Smith, P. Davey, S. Hennige, and N. R. Baker. 2008. Photosynthesis and production of hydrogen peroxide by *Symbiodinium* (Pyrrhophyta) phylotypes with different thermal tolerances. J. Phycol. **44:** 948–956, doi:10.1111/j.1529-8817.2008.00537.x

Sutton, D., and O. Hoegh-Guldberg. 1990. Host–zooxanthella interactions in four temperate marine invertebrate symbioses: Assessment of effect of host extracts on symbionts. Biol. Bull. **178:** 175–186, doi:10.2307/1541975

Takahashi, S., T. Nakamura, M. Sakamizu, R. Woesik, and H. Yamasaki. 2004. Repair machinery of symbiotic photosynthesis as the primary target of heat stress for reef-building corals. Plant Cell Physiol. **45:** 251–255, doi:10.1093/pcp/pch028

———, S. M. Whitney, and M. R. Badger. 2009. Different thermal sensitivity of the repair of photodamaged photosynthetic machinery in cultured *Symbiodinium* species. Proc. Natl. Acad. Sci. **106:** 3237–3242, doi:10.1073/pnas.0808363106

———, ———, S. Itoh, T. Maruyama, and M. Badger. 2008. Heat stress causes inhibition of the de novo synthesis of antenna proteins and photobleaching in cultured Symbiodinium. Proc. Natl. Acad. Sci. **105:** 4203–4208, doi:10.1073/pnas.0708554105

Tchernov, D., and others. 2004. Membrane lipids of symbiotic algae are diagnostic of sensitivity to thermal bleaching in corals. Proc. Natl. Acad. Sci. U. S. A. **101:** 13531–13535, doi:10.1073/pnas.0402907101

Titlyanov, E., and T. Titlyanova. 2002. Reef-building corals—symbiotic autotrophic organisms: 1. General structure, feeding pattern, and light-dependent distribution in the shelf. Russ. J. Mar. Biol. **28:** 1–15, doi:10.1023/A:1021836204655

Ulstrup, K., P. Ralph, A. Larkum, and M. Kühl. 2006. Intra-colonial variability in light acclimation of zooxanthellae in coral tissues of *Pocillopora damicornis*. Mar. Biol. **149:** 1325–1335, doi:10.1007/s00227-006-0286-4

Venn, A. A., J. E. Loram, and A. E. Douglas. 2008. Photosynthetic symbioses in animals. J. Exp. Bot. **59:** 1069–1080, doi:10.1093/jxb/erm328

———, M. A. Wilson, H. G. Trapido-Rosenthal, B. J. Keely, and A. E. Douglas. 2006. The impact of coral bleaching on the pigment profile of the symbiotic alga, Symbiodinium. Plant, Cell Environ. **29:** 2133–2142, doi:10.1111/j.1365-3040.2006.001587.x

Wang, J., and A. Douglas. 1999. Essential amino acid synthesis and nitrogen recycling in an alga–invertebrate symbiosis. Mar. Biol. **135:** 219–222, doi:10.1007/s002270050619

Wilkinson, C. [ed.]. 2002. Status of coral reefs of the world. Australian Institute of Marine Science.

Wooldridge, S. A., and T. J. Done. 2009. Improved water quality can ameliorate effects of climate change on corals. Ecol. Appl. **19:** 1492–1499, doi:10.1890/08-0963.1

Wyatt, A. S., R. J. Lowe, S. Humphries, and A. M. Waite. 2010. Particulate nutrient fluxes over a fringing coral reef: Relevant scales of phytoplankton production and mechanisms of supply. Mar. Ecol. Prog. Ser. **405:** 113–130, doi:10.3354/meps08508

Zhu, B., G. Wang, B. Huang, and C. Tseng. 2004. Effects of temperature, hypoxia, ammonia and nitrate on the bleaching among three coral species. Chin. Sci. Bull. **49:** 1923–1928.

Associate editor: Robert R. Bidigare

Received: 13 April 2013
Accepted: 17 October 2013
Amended: 19 November 2013